UNIVERSITY OF CALIFORNIA

Santa Barbara

Linking Seasonal Foliar Chemistry to VSWIR-TIR Spectroscopy Across California Ecosystems

A Thesis submitted in partial satisfaction of the

requirements for the degree Master of Arts

in Geography

by

Susan Kay Meerdink

Committee in charge:

Professor Dar Roberts, Chair

Professor Jennifer King

Professor Phaedon Kyriakidis

December 2014

The thesis of Susan Kay Meerdink is approved.

_____
Jennifer King

_____
Phaedon Kyriakidis

_____
Dar Roberts, Committee Chair

September 2014

Linking Seasonal Foliar Chemistry to VSWIR-TIR Spectroscopy

Across California Ecosystems

by

Susan Kay Meerdink

ABSTRACT

Linking Seasonal Foliar Chemistry to VSWIR-TIR Spectroscopy

Across California Ecosystems

by

Susan Kay Meerdink

Potential ecological impacts of disturbance, land use, and climate change have driven many studies to evaluate ecosystem functions through the measurement of vegetation biochemical properties that provide integral information on nutrient cycling, litter decomposition, and plant productivity. The use of spectroscopy in quantifying vegetation biochemistry shows promise with faster analytical speed than traditional methods. Synergies between the Visible Near Infrared/ Short Wave Infrared (VSWIR) and Thermal Infrared (TIR) spectra for identifying plant species' foliar chemistry have been largely unexplored. Here we evaluate the capability of VSWIR and/or TIR spectra to predict leaf levels of lignin, cellulose, nitrogen, water content, and leaf mass per area. We specifically examined how these predictive relationships might change seasonally and among plant functional types. Lastly we determined whether these relationships between spectra and foliar chemistry could be extended to the reduced spectral resolution available in airborne sensors, including the Airborne Visible/Infrared Imaging Spectrometer (AVIRIS), the Hyperspectral Thermal Emission Spectrometer (HyTES), and the combined AVIRIS and MODIS/ASTER

(MASTER) sensors used in the Hyperspectral Infrared Imager (HyspIRI) preparatory flight campaign.

In the 2013 spring, summer, and fall seasons, fresh leaves from sixteen common shrub and tree species in California representing three broad plant functional types were sampled from the Sierra Nevada Mountains, the Central Valley at the Sedgwick Reserve, and coastal Santa Barbara. Partial least squares regression (PLSR) analysis was used to relate spectral response at wavelengths from 0.3 – 15.4 μm to laboratory-measured biochemical and biophysical properties. For each component, three PLSR models were fit using different portions of the spectrum: VSWIR (0.3 – 2.5 μm), TIR (2.5 – 15.4 μm), and the full spectrum (0.3 – 15.4 μm). Three additional models were fitted using spectra resampled to AVIRIS (0.4 – 2.5 μm), HyTES (7.5 – 12 μm), and the combined AVIRIS and MASTER (0.38 – 12 μm).

The majority of the highest performing laboratory spectra models used either the TIR or full spectrum. When using simulated sensor spectra, the combined AVIRIS and MASTER produced the highest performing models, followed by HyTES. From both laboratory and sensor simulated model results, the combination of VSWIR and TIR increased the R^2 value of regression models compared to VSWIR alone, signifying that the inclusion of TIR data would improve predictions of foliar chemistry. We also found that model precision varied by seasons and across plant functional types. Models developed for all seasons resulted in a decreased R^2 value, but still had high precision ($R^2 > 0.85$) and accuracy (RMSE < 10%) when predicting cellulose, nitrogen, and water content. These results indicate that the TIR could augment the VSWIR in advancing identification of leaf properties of the world's ecosystems by helping to set the foundation for future use of the full spectrum represented by the proposed HyspIRI space-borne sensor.

TABLE OF CONTENTS

LIST OF FIGURES & TABLES

I. Introduction

Many studies aim at quantifying and characterizing ecosystem functions, especially with concern of the effects of climate, human disturbances, and land use (Ustin, 2013). Knowledge and understanding of these functions allow us to assess the health of an ecosystem. Vegetation characteristics such as chlorophyll, lignin, and nitrogen provide an insight into how ecosystems function through their role in nutrient cycling, gas exchange, and plant productivity (Curran, 1989; Townsend et al., 2003). However, traditional methods of collecting and processing vegetation characteristics on large scales for an extended period can be expensive and time consuming. Using relationships derived between spectra and laboratory measured components, imaging spectroscopy is an alternative method which shows promise in addressing these issues (Lawler et al., 2006).

To date, most spectroscopic studies have relied on only the Visible Near Infrared/Shortwave Infrared (VSWIR) spectrum to measure plant chemistry and biophysical properties. Laboratory VSWIR spectroscopy began in the field of agriculture to measure forage quality (Shenk et al., 1979), but has since been extended to other biochemical and biophysical properties of vegetation from the leaf to canopy scale. For example, Asner et al. (2011) used spectroscopy at 61 sites located in humid tropical forests to predict 21 leaf chemical properties with success ranging from an R^2 value of 0.62 – 0.88. Martin et al. (2008) developed canopy nitrogen prediction models for eight forests on four continents using NASA's Airborne Visible/Infrared Imaging Spectrometer (AVIRIS) and Hyperion instruments with the site-level R^2 values ranging from 0.69 – 0.85. Despite these achievements in predicting components, large portions of the VSWIR spectrum are obscured

by water and pigment absorption features, which hinder success in spectroscopic studies (Ribeiro da Luz and Crowley, 2010).

For this reason, studies have begun to use the Thermal Infrared (TIR) spectrum to answer questions about plant characteristics. Salisbury (1986) was the first to show that four plant species have spectral signatures that varied in the 8 – 14 μm range. However, use of the TIR in spectroscopic studies was not adopted as widely as the VSWIR due to low signal to noise ratio, limited availability of TIR sensors, and subtle features of plant spectra (Riberio da Luz and Crowley, 2007). More recently with technological advancements, Ullah et al. (2012a) showed that plant species from the Netherlands have spectral diversity in the mid wave infrared from 2.5 – 6 μm and the TIR from 8 –14μm, which could be used for species discrimination. Another study conducted by Fabre et al. (2011) found that leaf spectroscopy in the 3– 15 μm region was impacted by variations in leaf water content. These studies suggest that TIR could be utilized to improve species discrimination, thus opening doors to other applications such as quantification of biochemical properties. In fact, a study conducted by Ribeiro da Luz and Crowley (2007) found spectral features in the TIR (8 – 14 μm) associated with cellulose, cutin, xylan, silica, and oleanolic acid. Additionally, Ullah et al. (2014) used the full spectrum (0.39 – 14 μm) to retrieve leaf water content from eleven different plant species successfully. Integration of the VSWIR and TIR to cover a much larger range of wavelengths could allow researchers to utilize the strengths of each spectral region while minimizing limiting factors.

Very few studies have measured the full spectrum due to lack of sensors, but a satellite imaging spectrometer that measures 0.38 – 12 μm has been proposed by the National Aeronautic and Space Administration (NASA; Riberio da Luz and Crowley, 2007; Ullah et al. 2014). In 2013, NASA launched a preparatory campaign to determine if a satellite

imaging spectrometer known as the Hyperspectral Thermal Imager (HyspIRI) would be appropriate for studying ecosystem characteristics. A unique feature to this proposed mission is the inclusion of two instruments: an imaging spectrometer measuring the VSWIR spectrum and a multi-spectral imager measuring the TIR spectrum. This new spectrometer presents an opportunity to use a larger portion of the spectrum to address questions about ecosystem functions explained by biochemistry. Before determining if a satellite such as HyspIRI would in fact improve quantification of vegetation chemistry, a need exists to determine synergies between the VSWIR and TIR spectra.

The purpose of our study was to evaluate synergies between the VSWIR and TIR spectra for assessing plant species' foliar chemistry. Here we evaluate the capability of VSWIR and/or TIR spectra to predict leaf levels of lignin, cellulose, nitrogen, water content, and leaf mass per area (LMA). We specifically examined how these predictive relationships might change seasonally and among plant functional types. Lastly we determined whether these relationships between spectra and foliar chemistry could be extended to the reduced spectral resolution available in airborne sensors, including AVIRIS, the Hyperspectral Thermal Emission Spectrometer (HyTES), and combined AVIRIS and MODIS/ASTER (MASTER) sensors used in the HyspIRI preparatory flight campaign. We had three hypotheses for this study. First we hypothesized that spectra using the full spectral range would improve predictions of lignin, cellulose, nitrogen, water content, and LMA. Additionally, we predicted that one model created from all samples would provide high accuracy ($R^2 > 0.85$) to predict leaf components from all seasons and locations. We also hypothesized that the reduced spectral resolution of simulated sensors would retain high enough accuracy ($R^2 > 0.8$) to predict lignin, cellulose, nitrogen, water content, and LMA. To test these hypotheses, we compared partial least squares regression (PLSR) models using coefficient of

determination (R^2) and percent root mean squared error (RMSE %) created from different subsets of samples and regions of the spectrum.

II. Methods

A. Study Sites

We collected and analyzed plant samples from three different ecosystems located across California. The sites chosen provide a wide range of biochemistry and spectral values for analyses and represent a large change in elevation and ecosystem characteristics. Included in these analyses are the following sites: coastal Santa Barbara, Sedgwick Reserve, and Sierra Nevada Mountains (Figure 1).

The coastal Santa Barbara site was comprised of three sub-sites that surrounded the city of Santa Barbara, California to capture the diverse ecosystems of coastal California (Figure 1). These sub-sites were located at three elevations: 5, 515, and 1080 m. The lower elevation sub-site was located at the University of California Santa Barbara campus where we collected *Baccharis pilularis* (BAPI), a very common coastal shrub that does not grow at higher elevations (Table 1). The mid-elevation sub-site was located in the Santa Ynez Mountains, while the highest elevation sub-site was located in the Los Padres National Forest. Species collected at these sites include: *Adenostoma fasciculatum* (ADFA), *Arctostaphylos glandulosa* (ARGL), *Ceanothus cuneatus* (CECU), *Ceanothus megacarpus* (CEME), *Ceanothus spinosus* (CESP), *Heteromeles arbutifolia* (HEAR), and *Umbellularia californica* (UMCA). Many of these species and other dominant vegetation at these sub-sites are classified as chaparral, which is a product of the region's Mediterranean climate. These chaparral species form a nearly impenetrable thicket of shrubs with hard leaves and stiff

twigs, which makes them well adapted for the hot, dry summers and unpredictable precipitation during the winter (Quinn and Keeley, 2006). Most chaparral species are drought and fire adapted evergreen shrubs.

The Sedgwick Reserve site is located in the Santa Ynez Valley in Santa Barbara County, California (Figure 1). Created in 1996, the Sedgwick Reserve is the largest reserve managed by the University of California Natural Reserve System. With an annual precipitation of 38 cm, the three main vegetation communities are coastal sage scrub, oak woodland, and exotic grasses (Boot et al., 2013). Our sites within Sedgwick Reserve are located at elevations of 382 and 400 m. The lower elevation sub-site was the location of a large patch of *Salvia leucophylla* (SALE), while at the upper elevation sub-site *Quercus agrifolia* (QUAG), *Quercus douglasii* (QUDO), and *Quercus lobata* (QULO) were collected (Table 1).

The Sierra Nevada Mountains site is located in the Sierra National Forest at an elevation of 1400 m (Figure 1). At this elevation the site is composed of mixed conifer forest with shrub-dominated rocky outcrops (Dahlgren et al., 1997). We sampled four needleleaf evergreen species at this location: *Abies concolor* (ABCO), *Calocedrus decurrens* (CADE), *Pinus lambertiana* (PILA), and *Pinus ponderosa* (PILA) (Table 1). This area presents a much moister and cooler climate than our other study areas with an average of 101 cm of precipitation per year (Dahlgren et al., 1997).

B. Field Collection

We harvested a total of 288 samples from sixteen shrub and tree species common to the three areas (Table 1). Each species was represented by three individual plants that were stratified by season and leaf age. Each plant was sampled once during the 2013 spring, summer, and fall season with sampling dates timed to match HyspIRI airborne preparatory

flights (Table 1). During the fall season, due to the original plants being removed, three different BAPI plants were sampled. In all other cases, leaves were sampled from the same individuals each season. Because individual leaves may live for several years, but may change chemically over that time, leaves from each plant were divided into two age classes: the current year's new growth and previous year's growth. Leaf age was determined by leaf location on branch. Individual samples were composed of multiple randomly selected full-sun leaves because in all cases more than one leaf was needed to complete chemical and spectral analysis. A portion of individual samples were designated for lignin, cellulose, and water content, another for nitrogen and leaf mass per area (LMA), while the last was for spectroscopic analyses. The portion for spectroscopy and nitrogen analyses were placed in polyethylene bags with damp paper towels. These samples were then kept cool using an ice chest, and a towel was used to prevent from direct contact with ice. The portion destined for lignin, cellulose, and water content analyses were sealed tightly in a nalgene bottle.

C. Spectroscopy

Spectral response was measured at the NASA Jet Propulsion Laboratory within 48 hours of collection in order to preserve integrity of the samples. The VSWIR spectrum was obtained using an Analytical Spectra Device Full Range (ASD) spectrometer which covered the 0.3 – 2.5 μm range with a sampling interval of 1 nm (Analytical Spectra Devices, Inc., Boulder, CO USA). Spectralon was used as a calibrated reflectance standard to convert from raw radiance to reflectance (Labsphere Inc., Durham, NH). All samples were illuminated by a calibrated quartz halogen light source purchased from ASD, positioned at a 23 degree zenith angle and distance of 23 cm from the target. Spectra were collected using bare fiber (no foreoptic) with the fiber positioned at a 27 degree view zenith at a distance of 5 cm from

the target, producing a 1.5 cm diameter field of view. This configuration results in bi-directional reflectance with a 50 degree phase angle. All samples were collected with a < 5% reflectant black mat as a substrate to minimize substrate effects. Each set of spectra included five replicates, followed by rotation of the target and a second or third set of replicates depending upon heat loads. When applicable, spectra were collected of the upper and lower leaf surfaces. Here we only report reflectance from upper leaf surfaces.

The TIR spectrum was acquired using a Nicolet Model 520 Interferometer Spectrometer which measured from 2.5 – 15.4 μm with a sampling interval of 1 nm (Thermo Electron Corp., Madison, WI) . The spectrometer uses nitrogen gas to purge water vapor and carbon dioxide. Gold and distilled water were used as a TIR reflectance standard. Each spectrum was calculated from the average of 300 scans placing leaves on a tin foil to minimize substrate effects. In most cases leaves were clustered in order to obtain a large enough area to cover the field of view of both instruments. The full spectrum (0.3 – 15.4 μm) was obtained by combining the VSWIR and TIR spectra (Figure 2).

To test if the loss of spectral resolution would affect prediction of foliar properties, laboratory spectra were convolved to three sensors: AVIRIS, HyTES, and combined AVIRIS and MASTER. To simulate the AVIRIS sensor, VSWIR lab based measurements were convolved using a Gaussian model to 10 nm full-width half maximum bandwidth spanning 400 – 2500 nm (Green et al., 1998). In addition, to more closely simulate airborne measurements, the wavelengths falling within the 1350 – 1450 and 1850 – 1975 nm atmospheric water vapor regions were removed from AVIRIS simulated spectra (Gao and Goetz, 1995).

To simulate HyTES spectra, TIR lab based measurements were convolved using a Gaussian model to 256 spectral bands that ranged between 7.5 – 12 μm (Hook et al., 2013).

To determine the water vapor regions in this portion of the spectrum, H_2O transmittance was generated using MODTRAN for a sensor altitude of 1 km with a mid-latitude summer atmosphere. Wavelengths with less than 20% transmittance were removed.

To represent the full spectrum, the combination of AVIRIS and MASTER spectra were used because these sensors were flown on the HyspIRI preparatory flight campaign in 2013-2014 (Green et al., 2013). This flight campaign includes two instruments: an imaging spectrometer measuring 0.38 – 2.5 μm and a multispectral imager measuring from 3 – 12 μm. The imaging spectrometer used is the AVIRIS sensor, while the multispectral imager used is the MODIS/ASTER (MASTER) airborne sensor (Hook et al., 2001). To obtain the MASTER spectrum, the TIR spectrum was convolved using a Gaussian model to MASTER's 25 channels from 2.5 – 12.876 μm. The combined AVIRIS and MASTER spectra will be referred to as AVIRIS + MASTER or AVMA throughout.

D. Biochemistry

Lignin and cellulose were analyzed using a sequential acid digestion lignin procedure with the Ankom Fiber Digestion Analyzer (ANKOM, Fairport, NY, USA). This method has been used in a diversity of studies to evaluate lignin and cellulose concentrations (Hatfield and Fukushima, 2005; Lawler et al. 2006). For this method, samples are oven-dried at 60˚C for at least 48 hours and ground using a 1 mm (20 mesh Wiley mill) screen. Sample weights for analysis were approximately 0.5 g.

Leaf water content was calculated using the formula from Ullah et al. (2014): leaf water content = $100(Mw - Md)/Mw$, where Mw is the mass of the wet leaf and Md is the mass of the completely dried leaf. Fresh leaf samples were weighed both before and after being dried at 60˚C for at least 48 hours.

To obtain LMA, enough leaves were used to cover a sheet of white 8.5x11 inch paper. These samples were photographed and placed into a nalgene bottle. Samples were oven-dried at 70˚C for 72 hours and weighed. ImageJ software was used to measure leaf area of photographed samples (Schneider et al., 2012).

After LMA analysis, samples were then ground into a fine, homogeneous powder using a roller milling device for nitrogen analysis (Arnold and Schepers, 2004). Nitrogen content was obtained using a combustion method with the NA 1500 Series 2 Nitrogen and Carbon analyzer (COSTECH Analytical, Valencia, CA). This method is efficient for determining nitrogen concentration in plants with high precision compared to other methods (Da Silva Dias et al., 2013). Sample weights for analysis were approximately 8 mg. A one-way ANOVA was used to determine whether or not leaf lignin, cellulose, nitrogen, water content, and LMA for each species varied significantly throughout all three seasons (Table 3).

E. Statistical Methods

We analyzed relationships among spectra and lignin, cellulose, nitrogen, water content, and LMA using the partial least squares regression (PLSR) method. This method is similar to traditional regression models because a linear multivariate model is used to relate two data matrices, X and Y (Haaland and Thomas, 1988). However PLSR's ability to analyze data with many, noisy, correlated variables in both X and Y separates this method from traditional regression methods (Wold et al., 2001). PLSR has been used in many spectroscopic studies and shows consistently high R^2 values compared to other commonly used methods (Bolster et al., 1996; Doughty et al., 2011; Ferwerda et al., 2005; Martens et al., 1987).

We used reflectance spectra as the independent variables instead of first or second derivative spectra which have been suggested in the literature (Townsend et al., 2003). To determine the number of factors for each regression we used leave-one-out cross validation. This method reduces the possibility of over fitting the model with too many factors and produces a predicted residual error sum of squares (PRESS) statistic for total number of factors. The model with the minimum PRESS statistic is considered to have the optimum number of factors (Martens et al., 1987). If there was a local minimum of the PRESS statistic in addition to global minima, the lowest number of factors was chosen.

Models were validated by holding out 10% of the data during each iteration, until all samples had been removed once. To determine the performance of the models, predicted components from the spectra were compared to laboratory measurements of its corresponding component using R^2 and RMSE % to report the accuracy of the models. RMSE % was used to enable model comparison across leaf components, as it is normalized by the percentage of the response data range (Feilhauer et al., 2010). Models were considered to have high precision if $R^2 > 0.75$ and high accuracy if RMSE < 15% (Asner et al., 2011).

We developed an equation using all samples collected and compared this to equations developed for seasons and functional types to determine whether predictive relationships might change seasonally and among plant functional types. The seasonal equations were divided into samples collected in the spring, summer, and fall. The functional type equations were divided into broadleaf deciduous, broadleaf evergreen, and needleleaf evergreen (Table1). In summary, samples were divided into seven model classes for each component: All Samples (AS), Spring, Summer, Fall, Broadleaf Deciduous (BD), Broadleaf Evergreen (BE), and Needleleaf Evergreen (NE).

Each model class was run six times with a different region of the spectrum: VSWIR, TIR, Full, AVIRIS, HyTES, and AVIRIS + MASTER. Three regression models were fitted using different portions of the available laboratory spectrum: VSWIR spectrum (0.3 – 2.5 μm), TIR spectrum (2.5 – 15.4 μm), and the full spectrum (0.3 – 15.4 μm). Finally, to test if these relationships could translate to larger scale remote sensing applications, three more regression models were fitted using simulated spectra from three sensors: AVIRIS, HyTES, and AVIRIS + MASTER (AVMA). Individual models will be referred to throughout this paper as model_spectrum. For example, the model created using only broadleaf deciduous plant functional type samples and the AVIRIS + MASTER spectrum will be referenced as BD_AVMA.

III. Results

A. Lignin

For all species, lignin content varied from 2.6 – 22.5% and had a mean of 10.3% with a standard deviation of 3.4% (Table 2). On average, these values are generally lower than values reported in other studies due to our method of measuring lignin. There is a discrepancy between lignin determination methods because lignin is not easily quantified within various types of plant material (Hatfield and Fukushima, 2005). Currently there is not a preferred lignin determination method, but the sequential digestion method is known to produce lower lignin concentrations (Hatfield and Fukushima, 2005).

Throughout the year, species' lignin content varied by seasons. The following species had the highest lignin content in the fall season ($p < 0.05$): CADE, CECU, CESP, PILA, PIPO, and QULO (Table 3; Figure A1). The increased lignin content in sampled leaves can

be explained by the fact that lignin concentration increases as these leaves lignify with age (Martin and Aber, 1997). Not all species followed this pattern. BAPI had the highest lignin content in the summer ($p < 0.01$), but the pattern may not hold true due to the fall season samples being collected from different shrubs. HEAR was unique in that lignin content was similar for spring and summer, but the fall season showed a decrease ($p = 0.004$).

The models predicting percent lignin had R^2 values ranging from 0.40 – 0.90. The number of factors ranged from 4 – 23 and the RMSE ranged from 6.11 – 10.58% (Figure 2; Table A1). At first glance, two model classes stand out as having the lowest precision ($R^2 < 0.6$) across all spectra: All Samples (AS) and Needleleaf Evergreen (NE). On the other hand, one of the best model classes was Broadleaf Deciduous (BD), which was predicted well ($R^2 > 0.9$) for most spectral divisions. The consistently high prediction of lignin in BD could be contributed to the smaller amount of variation in lignin content for these species compared to other plant functional types. When predicting leaf lignin content, no spectrum domain was top performing for all model classes. In general, most models had fewer than 10 components. Outliers included the AS_Full, BE_VSWIR, and BE_AVIRIS models. The models using the TIR spectrum consistently had a lower number of factors compared to other spectra. This same pattern is true for simulated sensor spectra where the HyTES spectrum had the lowest number of factors.

The highest precision model for each model category using laboratory spectra to predict lignin are ranked from high to low as BD_Full, BE_VSWIR, Summer_TIR, Spring_Full, Fall_TIR, NE_Full, and AS_Full (Table 4). For the laboratory-based spectra, the division of samples into seasons or functional types increased the precision of predicting lignin compared to models created from all samples. By dividing the samples by season, a more consistent prediction was achieved with R^2 values ranging from 0.82 – 0.89 and RMSE

ranging from 6.54 – 9.12%. For samples divided up by season, the TIR spectrum appears to be important in quantifying lignin. The division of samples into functional types resulted in higher precision, compared to the seasonal division, for two of the three functional types. The lignin content of NE was not easily predicted. On the other hand BE model had high precision, but also used 23 factors, which is twice the number of factors as the other models.

The models using sensor simulated spectra to predict lignin are ranked from high to low as: Spring_HyTES, BD_AVMA, Summer_HyTES, Fall_HyTES, NE_HyTES, BE_HyTES, and AS_HyTES (Table 5). In all categories, except for the broadleaf deciduous plant functional type, the best models used wavelengths associated with the HyTES sensor. Dividing the samples into seasonal models resulted in the highest precision compared to the AS model. The division of samples into plant functional types also improved prediction, but not as much as the seasonal division. While some precision was lost with the reduction of spectral resolution, lignin was still predicted with high precision (R^2 >= 0.8) using the HyTES spectrum if samples were analyzed by season or plant functional type.

To determine whether the models identified known absorption features of lignin, regression coefficients for AS_VSWIR, AS_TIR, and AS_Full models were plotted in relation to the average reflectance spectrum (Figure 3). In addition this figure shows the corresponding precision of the AS_VSWIR, AS_TIR, and AS_Full models through the predicted versus laboratory measured lignin plots. The wavelengths related to the four largest regression coefficients and the structures associated with those wavelengths were identified for VSWIR, TIR, and full spectrum (Table 6). The VSWIR and TIR spectra models identified absorption features not necessarily related to lignin, but other components such as starch, protein, and wax. The full spectrum's largest coefficients identified wavelengths in the TIR spectrum that are known absorption features of either lignin or

cellulose. The AS_Full model had the highest precision of this model class and also identified the most wavelengths directly related to lignin absorption features.

B. Cellulose

Percent cellulose for all species ranged from 4.20 – 27.33% and had a mean of 11.82% with a standard deviation of 4.81% (Table 2). CESP had the lowest mean cellulose content, while QUAG had the highest mean. In general most species' cellulose content remained consistent throughout the year, but a few species had variations from season to season. Six species had statistically significant variations in cellulose content over time (Table 3; Figure A2). ADFA, PILA, PIPO, and UMCA had the highest cellulose content in the fall ($p < 0.05$). The fall samples of BAPI had the lowest cellulose content, but since a new set of shrubs was collected for the fall season, this result may not be caused by a seasonal change ($p = 0.03$). CECU was unique in that it was the only species that had significantly higher cellulose content in summer as opposed to fall and spring ($p = 0.002$).

The R^2 values for cellulose predictions ranged from 0.26 – 0.98, the number of factors ranged from 4 – 34, and RMSE ranged from 3.32 – 11.61% (Figure 4; Table A1). Cellulose prediction models did very well ($R^2 > 0.9$) across the majority of models using laboratory spectra. While prediction models using simulated sensor spectra did not do as well as the laboratory spectra, most models still performed well as defined by the threshold of $R^2 > 0.75$. One of the only exceptions was the broadleaf deciduous plant functional type, which only achieved R^2 values of approximately 0.75 for all laboratory and simulated sensor spectra. The last exception was the TIR and HyTES, which had accuracies below 0.75 for most models. All models created with the TIR, HyTES, and broadleaf deciduous plant

functional type had the lowest number of factors. The models using the highest number of factors were the AS_VSWIR and AS_AVIRIS models (Table A1).

For laboratory spectra, the models are ranked from high to low as Summer_TIR, NE_VSWIR, AS_VSWIR, BE_Full, Spring_Full, Fall_VSWIR, and BD_Full (Table 4). The AS_VSWIR model had high precision, but required approximately twice the number of factors to explain the variation. When samples were divided into seasons or functional types, the number of factors required for the model decreased but the precision did not. Each season used a different portion of the spectrum with similar accuracies and factors. As for the division of samples into functional types, BE_Full and NE_VSWIR performed on par with the AS_VSWIR model. However, BD_Full had the lowest R^2 value of all models using the laboratory spectra. When predicting cellulose using laboratory spectra, the VSWIR and full spectrum had the highest performing models.

Translating this to sensor simulated spectra, the ranking of models from high to low changes to: NE_AVIRIS, Summer_AVMA, AS_AVIRIS, Fall_AVMA, BE_AVMA, Spring_HyTES, and BD_HyTES (Table 5). Three of the seven models used AVIRIS + MASTER, while the other four models were evenly split between AVIRIS and HyTES spectra. The AS model used the AVIRIS spectrum with high precision of $R^2 = 0.93$, but again required the most number of factors to explain the variance. These models decreased in precision slightly compared to laboratory wavelength ranges, but the sensor simulated spectra retain a high enough spectral resolution to predict cellulose content.

The AS model regression coefficients for VSWIR, TIR, and full spectrum were plotted in relation to the average reflectance spectrum to determine whether the models were associated with known absorption features of cellulose (Figure 5). The precision, shown through predicted versus measured cellulose, of the resulting models are shown next to the

corresponding regression coefficients (Figure 5). The wavelengths related to the four largest regression coefficients and the structures associated with those wavelengths were identified for VSWIR, TIR, and Full spectrum (Table 6). The regression coefficients from the TIR model included wavelengths directly related to cellulose absorption features. The Full spectrum model also included wavelengths related to cellulose absorption, but did not perform as well as the TIR model. The VSWIR model used the least number of wavelengths associated with cellulose, but chose absorption features related to protein, starch, and .CH_2. This model had the highest precision, but also needed more than twice the number of components compared to the TIR to explain the variance.

C. Nitrogen

For all samples, nitrogen content ranged from 0.45 – 3.81% with a mean of 1.4% and standard deviation of 0.6% (Table 2). ARGL had the lowest mean nitrogen content, while BAPI had the highest. Throughout the year, nitrogen changed from season to season for most species. The following species have nitrogen content that were statistically differed by season ($p < 0.05$): ADFA, BAPI, CEME, PIPO, QUDO, QULO, and SALE (Table 3; Figure A3). In general these species had higher nitrogen content in the spring season. The only exception is PIPO, where the summer season had the highest amount of nitrogen. In general, the needleleaf evergreen tree species did not vary much in nitrogen content, compared to other functional types.

The models' R^2 values for nitrogen predictions ranged from 0.35 – 0.96, the number of factors ranged from 4 – 26, and RMSE ranged from 4.70 – 12.25% (Figure 6; Table A1). The broadleaf deciduous plant functional type had the highest precision across all spectra except for the TIR. The fall season was not predicted well by most spectra ($R^2 < 0.65$), with

the only exception being the TIR spectrum ($R^2 = 0.90$). All other models had a very similar number of factors, excluding the AS and BE models which had the highest number of factors.

For laboratory spectra, the models are ranked from high to low as: BD_Full, Spring_Full, Fall_TIR, NE_TIR, AS_VSWIR, Summer_TIR, and BE_VSWIR (Table 4). All highest performing models predicted nitrogen content well ($R^2 > 0.8$). The AS model used more than double the number of factors. By dividing up samples into seasons or functional types, fewer factors were needed because there was less variation in the dataset. In most cases this also improved the precision of the model. Models using the TIR spectrum required fewer factors to explain the variation compared to the VSWIR or full spectrum. When predicting nitrogen using laboratory spectra, our models had the highest precision if they incorporated the TIR spectrum either through the full spectrum or stand alone.

For sensor simulated spectra, the models are ranked from high to low as BD_HyTES, Spring_AVMA, AS_AVIRIS, NE_HyTES, BE_AVMA, Summer_AVIRIS, and Fall_AVMA (Table 5). Switching to wavelengths associated with known or proposed sensors decreases the prediction of nitrogen, but models still retain R^2 values above 0.8 except for the summer or fall season. The TIR spectrum, by way of HyTES, is not as widely implemented in the best models as in the laboratory spectra models, although the model with the highest R^2 value was predicted using the TIR spectrum and broadleaf deciduous functional type. With the decrease of spectral resolution, the AS_AVIRIS model is ranked higher and would be more appropriate for predicting nitrogen.

Regression coefficients for VSWIR, TIR, and full spectrum AS models were graphed in relation to the average reflectance spectrum to determine whether the models detected known absorption features of nitrogen (Figure 7). The precision of nitrogen prediction using

the resulting models are shown next to the corresponding regression coefficients (Figure 7). The wavelengths related to the four largest regression coefficients and the structures associated with those wavelengths were identified for VSWIR, TIR, and full spectrum (Table 6). The AS_VSWIR model had the highest precision compared to the TIR or full spectrum. This was also the only model to identify absorption features related to nitrogen specifically. All other models identified wavelengths related to absorption features of cellulose or lignin.

D. Water Content

Water content ranged from 20.22 – 76.85% for all sixteen species with a mean of 51.0% and standard deviation of 9.3% (Table 2). Throughout the year, water content varied by season for almost all species. The following species did not have a significant change in water content by season ($p > 0.05$): CADE, PIPO, and QUAG (Table 3; Figure A4). The other thirteen species had a least one season in which water content values were statistically significant. All species collected from the Santa Barbara area had lower water content in the fall season, which corresponds to the driest time of year for the area. In addition, for species collected from the Sedgwick Reserve we observed a large decrease in water content as the seasons progressed from spring to summer to fall. The only exception was QUAG, a broadleaf evergreen tree species, where foliar water content was fairly consistent throughout the year. Species collected in the Sierra Nevada Mountain range had the highest water content in the fall.

The R^2 value for water content predictions ranged from 0.29 – 0.99, the number of factors ranged from 5 – 19, and RMSE ranged from 2.6 – 11.21% (Figure 8; Table A2). Water content models exceeded the threshold of a good prediction model as $R^2 > 0.85$ for

almost all models and all spectra. The exceptions were a few models using the TIR or HyTES spectrum, where eight of the fourteen models had low precision. The broadleaf deciduous plant functional type had high precision for all spectra with models exceeding the threshold of $R^2 > 0.75$. The number of factors used in each model were consistent, except for the AS models with 25 factors.

Ranked by high to low precision, the models using laboratory spectra are: Spring_TIR, BD_TIR, Fall_TIR, NE_TIR, BE_Full, Summer_Full, and AS_Full (Table 4). The four highest ranked models used the TIR spectrum, while the lowest three utilized the full spectrum. The use of the TIR spectrum, compared to the full spectrum, did reduce the number of factors used to create the model, showing that the TIR spectrum can explain the same amount of variance with fewer factors for water content. The best models using laboratory spectra had very high precision with an R^2 value above 0.9. The model created from AS ranked low compared to the season or functional type models, but still had an R^2 value of 0.92.

For sensor simulated spectra the best models for each category are ranked as: BD_HyTES, AS_AVMA, BE_AVMA, Summer_AVMA, Spring_AVIRIS, Fall_AVMA, and NE_AVMA (Table 5). In general the predictive power is reduced compared to laboratory spectra, but still retains high precision with R^2 values that are above 0.86 for the best models in each category. The AVIRIS + MASTER spectrum is used most often in the best models instead of the TIR which was used predominately in the laboratory spectra. The model constructed using AS had the second highest ranked R^2 at 0.93, which is higher than the AS model using the laboratory spectra.

Regression coefficients for AS_VSWIR, AS_TIR, and AS_Full models were plotted in relation to the average reflectance spectrum to determine whether the models distinguished

wavelengths related to known absorption features of water content (Figure 9). The precision of water content predictions using the resulting models are shown next to the corresponding regression coefficients (Figure 9). The wavelengths related to the four largest regression coefficients and the structures associated with those wavelengths were identified for VSWIR, TIR, and full spectrum (Table 6). The TIR model's largest coefficients were related to water content absorption features. The VSWIR and full spectrum also had a large coefficient based on one water absorption feature, but also used wavelengths that correspond to cellulose, lignin, starch, chlorophyll b, and urea.

E. LMA

Leaf mass per area (LMA) varied from 0.4 – 7.13 g/m^2 for all sixteen species with a mean and standard deviation of 2.34 and 1.39 (Table 2). Species showed slight variations in LMA from season to season. The following species had a statistically significant change in LMA by season ($p < 0.05$): BAPI, CADE, CECU, CEME, PIPO, QUAG, QUDO, and SALE (Table 3; Figure A5). In general BAPI had the lowest LMA, while PIPO had the highest values. The summer collection of PIPO showed the largest variation, which corresponds to the new growth occurring at this time ($p = 0.048$). This pattern is similar for ADFA, CADE, and CECU where a clear distinction in the spring season occurs between new leaves and old leaves. The fall collection of BAPI had the lowest LMA ($p = 0.009$); however, since a new set of shrubs were collected for the fall season, this may not be caused by a seasonal change.

The R^2 for LMA predictions ranged from 0.47 – 0.98, the number of factors ranged from 3 – 12, and RMSE ranged from 3.03 – 12.81% (Figure 10; Table A2). The TIR spectrum yielded the best model results ($R^2 > 0.8$) compared to other spectra.These results did not translate to the reduced spectral resolution of the HyTES sensor, with only summer and

broadleaf deciduous plant functional type achieving an $R^2 > 0.8$. In general the AS models for all spectra produced less precise and accurate models compared to seasonal or plant functional type models. All models had a similar number of factors and a relatively small range compared to other biochemical properties in this paper.

Ranked by R^2 value from high to low, the best models for each category using laboratory spectra are: Fall_TIR, Summer_TIR, BE_TIR, BD_TIR, Spring_VSWIR, AS_Full, and NE_Full (Table 4). The top four best models for each category used the TIR spectrum. The AS_Full model was the second lowest performing model. For predicting LMA with laboratory spectra, the AS_Full model had a low precision ($R^2 = 0.78$) while dividing samples by season or plant functional type generally resulted in the highest R^2 value. However, compared to other models the NE_Full model has a lower precision ($R^2 = 0.76$) and accuracy (RMSE = 9.95%) when predicting LMA.

Ranked by R^2, the best models for each category using sensor simulated spectra are: BD_HyTES, Summer_AVMA, Spring_AVMA, BE_AVMA, AS_AVMA, Fall_AVIRIS, and NE_HyTES (Table 5). Transitioning to sensor simulated spectra, the majority of the top performing models used the AVIRIS + MASTER spectrum. All other models' precision suffered with decreased spectral resolution except for the BD model, for which the R^2 increased from 0.83 using the TIR spectrum to 0.98 using the HyTES spectrum. Dividing samples up into seasons or functional types along with using the AVIRIS + MASTER spectrum improved prediction of LMA in most cases compared to the AS model.

Regression coefficients for AS_VSWIR, AS_TIR, and AS_Full models were plotted in relation to the average reflectance spectrum to determine whether the models identify known absorption features (Figure 11). The precision of LMA prediction using the resulting models are alongside to the corresponding regression coefficients (Figure 11). The wavelengths

related to the four largest regression coefficients and the structures associated with those wavelengths were identified for VSWIR, TIR, and full spectrum (Table 6). While LMA does not have any specific absorption features, other biochemical absorption features were identified. The full spectrum's largest regression coefficients were associated with cellulose, CH_2, and humic acid. The VSWIR model uses wavelengths associated with water, cellulose, starch, lignin, chlorophyll a, and aromatics. The TIR model, which had the highest precision of the AS models, used features related to lignin, water, cellulose, and humic acid.

IV. Discussion

A. Lignin

The majority of the highest precision models for predicting lignin use the full spectrum at fine spectral resolution and the HyTES spectrum at coarser spectral resolution. The VSWIR and AVIRIS spectra were not prominently used in predicting lignin, while the TIR and HyTES spectra were used frequently in models with the highest precision. This is related to the majority of known lignin absorption features residing in wavelengths 2.5 – 13 μm (Elvidge, 1988). Of these absorption features, the strongest and largest lie in the mid-infrared range of 2.5 – 6 μm (Elvidge, 1988). We see this in the largest regression coefficients of the AS_Full model.

With reduced spectral resolution, the precision of predicting lignin decreased for most model classes. The larger bandwidths that are used in the sensor simulated data are not able to capture the subtle spectral features that are related to lignin. However, prediction accuracies still retain an $R^2 > 0.75$ and RMSE < 10% which are classified as above the good prediction model threshold, except for the AS model. The AVIRIS + MASTER model for AS, spring, BD, and NE outperformed the AVIRIS model, showing that although the

AVIRIS + MASTER spectrum contains only 25 wavelengths in TIR, these still improve predictions of lignin for these classes.

Our model results are in line with other studies' lignin prediction results. The lowest performing model (AS model with $R^2 = 0.59$ and RMSE = 6.20%) is similar to Asner et al. (2011), where model results were an R^2 value of 0.62 and RMSE of 10.0% for plants located at 61 sites distributed throughout the world. Martin and Aber (1997) developed models with a prediction precision of $R^2 = 0.77$. Models reached accuracies of $R^2 > 0.8$ and RMSE < 10% when samples were divided into groups such as by season or plant functional type. When samples were divided into seasons, model accuracies more closely resembled studies such as Bolster et al. (1996) where samples were mostly collected in June 1992 and included 25 deciduous and 14 conifer species (Bolster et al., 1996). Their final models had a precision of $R^2 = 0.88$, which reflects our seasonal model results that ranged from R^2 of 0.82 – 0.89.

B. Cellulose

For cellulose content prediction, the top performing models for laboratory spectra models used the VSWIR and full spectrum. For sensor simulated spectra, the majority of the top performing models chose the AVIRIS + MASTER spectrum. While model precision decreased with spectral resolution, our models found that the wavelengths available in the AVIRIS + MASTER sensors are still able to predict cellulose contents with high precision ($R^2 > 0.75$) and high accuracy (RMSE < 10%), above the good prediction model threshold. Additionally, the AVMA's TIR spectrum contributed to a higher prediction of cellulose content compared to just the AVIRIS sensor for spring, summer, fall, BD, and BE. For both resolutions, the AS models had both high precision ($R^2 > 0.9$) and high accuracy (RMSE < 8%). While, dividing samples into seasonal and plant functional types did not improve

model accuracy and precision. Cellulose forms one third to one half of the dry weight in most plants making it the most abundant organic compound in terrestrial ecosystems (Elvidge, 1988). This may contribute to a larger spectral signal related to cellulose that allows this component to be predicted using the AS models and with higher accuracies compared to other components such as lignin and nitrogen.

A larger number of factors are needed in the models to predict cellulose content compared to lignin, nitrogen, LMA, and water content. The VSWIR and AVIRIS models required the largest number of factors and had the best cellulose prediction models. However, the majority of the top performing models used portions of the TIR spectrum which is consistent with other studies (Ribeiro da Luz, 2006; Ribeiro da Luz and Crowley, 2007). Cellulose is one of the few components being analyzed using the TIR spectrum because of strong absorption features in this region (Ribeiro da Luz and Crowley, 2007).

Our model results are similar to other studies that have predicted foliar cellulose content. For fresh leaf samples, Asner et al. (2011) reported a precision using AVIRIS simulated spectra of $R^2 = 0.77$, and Bolster et al. (1996) reported a precision of $R^2 = 0.89$. While most of our models reported higher accuracies than models measuring fresh leaf samples, a study done by Kokaly and Clark (1999) found coefficients of determination from 0.75 – 0.93 for dried leaf samples.

C. Nitrogen

Known absorption features related to nitrogen are located in the VSWIR spectrum (Curran, 1989). However in our study we found that the majority of the best performing models for predicting nitrogen used the TIR spectrum at fine spectral resolution. The model classes that chose TIR were summer, fall, and needleleaf evergreen plant functional type.

These sample divisions have the lowest amount of nitrogen, suggesting that at low nitrogen content, models that use the TIR spectrum maybe more useful compared to the VSWIR. The largest regression coefficients for the TIR spectrum relate to structural leaf components such as lignin and cellulose (Elvidge, 1988).

Of all biochemical and biophysical components analyzed in this thesis, nitrogen model precision was reduced the most by the lower spectral resolution of the sensor simulated spectra. A possible reason could be that spectral features related to nitrogen are masked with the averaging of bands over a larger width. The majority of the best performing models for predicting nitrogen used the AVIRIS + MASTER spectrum at coarser spectral resolution. For some model classes, reduction of spectral resolution reduced nitrogen prediction precision, such as the fall season which had a prediction precision of $R^2 = 0.90$ and dropped to 0.56. The Fall_AVMA and Summer_AVIRIS models, while the best for these seasons still had the lowest performance compared to other models. This could be caused by leaf senescence that was occurring for many species during these seasons creating a large variation in nitrogen that the models are not able to capture. When predicting nitrogen content, our study found that the AS_AVIRIS model produced a high precision ($R^2 = 0.86$) and high accuracy (RMSE = 7.82%), which was better than the majority of models where the samples were divided into seasons or plant functional types. Adding wavelengths in the TIR spectrum to AVIRIS contributed to higher predictions for AVIRIS + MASTER models compared to AVIRIS models for spring, fall, BD, BE, and NE.

Nitrogen prediction models have a wide range of precision over many studies. Other studies reported model accuracies ranging from R^2 values of 0.75 – 0.97 (Bolster et al., 1996; Dury and Turner, 2001; Huang et al., 2004; Smith et al., 2003; Yoder and Pettigrew-Crosby, 1995). On the lower end, Asner et al. (2011) reported a nitrogen prediction result of

R^2 = 0.77. In the middle range, Martin and Aber (1997) modeled prediction of seasonal variation of foliar nitrogen and found a model precision of R^2 = 0.87. The highest PLSR model result for nitrogen prediction was an R^2 = 0.97 from Bolster et al. (1996). These studies encompass our model results, which ranged from R^2 values of 0.71 – 0.92. While our model results fall into the range reported by other studies, discrepancies may be a result of the leaf nitrogen content of species sampled. Our study had lower mean nitrogen content averaged for all species compared to the studies mentioned above (Asner et al., 2011; Bolster et al., 1996; Martin and Aber, 1997)

D. Water Content

Our leaf water content prediction models had high precision with R^2 values above 0.86 and had the highest model accuracies compared to lignin, cellulose, nitrogen, and LMA. In fresh green leaves, water is a major constituent and can account for 40 – 80% of weight (Elvidge, 1988). This could result in a larger spectral signal of water that models were able to capture and result in higher prediction accuracies compared to other components that account for a smaller portion of leaf composition. When predicting water content, the AS_AVMA model produced a very high precision (R^2 = 0.93), outperforming many of the seasonal or plant functional type model classes. The literature supports this high accuracy model for prediction of water content. Asner et al. (2011) and Asner and Martin (2008) using AVIRIS simulated spectra reported a prediction R^2 value of 0.88 and 0.91, respectively. Curran at al. (2001) reported an even higher model result of 0.94 for slash pine needles. All of these studies used the VSWIR spectrum to obtain water content predictions.

In our study, top performing models predicting water content used the TIR spectrum at fine spectral resolution and the AVIRIS + MASTER spectrum at coarser spectral resolution.

For the prediction of water content, the TIR spectrum was beneficial to the model precision, as all but one of the highest performing models for laboratory and sensor simulated spectra used the TIR alone or the full spectrum. This is true even for the reduced spectral resolution of the AVIRIS + MASTER spectra in the TIR region, where all but one model class had this spectrum as performing better than the AVIRIS spectrum alone. This agrees with newly released studies that have analyzed foliar water content in the TIR spectrum. For example, a couple studies examined how leaf spectral signatures change with variations of leaf water content and found that in the 3 – 5.5 μm region spectral signatures are increasingly sensitive to leaf water content (Fabre et al., 2011; Ullah et al., 2012b; Ullah et al., 2013). More recently Ullah et al. (2014) analyzed leaf water content in different portions of the full spectrum (0.39 – 14.0 μm) by running PLSR models. The final models predicting leaf water content contained a similar number of factors (8, 9, and 10) to our final models. The MIR (2.5 – 6 μm) spectral region resulted in the highest $R^2 = 0.96$, which corresponds to the same region that contained the highest regression coefficients of our models.

E. LMA

The TIR spectrum at fine spectral resolution and the AVIRIS + MASTER spectrum at coarser spectral resolution was used in the majority of the highest precision models for predicting LMA. Model precision decreases at the lower spectral resolution, especially for some model classes more than others. For example, the Fall model prediction went from the highest performing of the laboratory spectra at $R^2 = 0.98$ to one of the lowest performing using the AVIRIS spectrum at an R^2 value of 0.74. Additional TIR wavelengths available in the AVIRIS + MASTER spectrum improved accuracy compared to the AVIRIS spectrum alone, showing that the TIR spectrum played a role in predictions of LMA.

Including both the laboratory and sensor simulated spectra, the AS model did not perform as well as the seasonal models. The plant functional types were expected to perform better than seasonal models because LMA are most easily explained by functional groups (Poorter et al., 2009). However, the plant functional type models had the lowest and highest accuracies ranging from NE with $R^2 = 0.66$ to BD with $R^2 = 0.98$. These results might be explained by the needleleaf evergreen plant functional type having twice the range of LMA values compared to the other plant functional types. This wide range of LMA could be attributed to aging of leaves as they were collected during the three seasons and result in the model's inability to accurately capture this wide variation.

In our study the sensor simulated spectra models had an R^2 value ranging from 0.66 – 0.98. Many studies do not report R^2 values as low as some of our models, but there are many to support the higher accuracies with R^2 values generally ranging from 0.8 – 0.9 (Asner et al., 2009; Asner et al., 2011; Asner and Martin, 2008; Doughty et al., 2011). All of these studies used the VSWIR, while we achieved similar accuracies using the AVIRIS + MASTER or HyTES simulated spectra.

F. Considerations for HyspIRI

To harness the temporal and spatial scale that is available using aerial and space-borne sensors, a generalized and transportable model should be developed to map canopy biochemical and biophysical properties (Asner et al., 2011). We tested the feasibility of this for three California ecosystems when developing the AS model which incorporates all seasons and plant functional types. The AS models using AVMA or AVIRIS spectra predicted cellulose, nitrogen, and water content at high accuracies ($R^2 > 0.85$) and precisions (RMSE < 8%). These models are considered to have high precision because $R^2 > 0.75$ and

high accuracy because RMSE < 15% (Asner et al. 2011).When predicting LMA and lignin, the AS_AVMA model had moderate success with an accuracy of $R^2 = 0.75$ and 0.58, which might not be suitable for prediction over many seasons and plant functional types. By dividing LMA and lignin prediction models into seasons, the accuracy of model predictions increased above a R^2 value of 0.80 suggesting that separate equations may be needed for different seasons for LMA.

While simulated sensor models assess how well reduced spectral resolution can discriminate foliar components, there are other considerations to be made when up-scaling to canopy level spectroscopy using a full spectrum satellite sensor such as the proposed HyspIRI sensor. The impact of spatial and temporal resolution on our ability to predict vegetation properties at this level is still being researched. Using full spectrum spectroscopy on a global scale poses several challenges caused by the atmosphere, lighting geometry, temperature-emissivity separability, canopy structure, and variability of vegetation characteristics. In a laboratory there is a controlled environment and lighting geometry, but spectral reflectance measurements are sensitive to a variable atmosphere and light geometry that fluctuates by time of year and location. While we attempted to correct for the atmosphere's effect by removing water vapor regions of the spectrum, ultimately there is still enough interference from the atmospheric attenuation and emission to obscure surface spectra (Young et al., 2002). Temperature variations, leaf angle, and shading inside a canopy would complicate emissivity retrievals, which need to be retrieved using atmospheric compensation and temperature-emissivity separation methods (Ribeiro da Luz and Crowley, 2010). Our study attempted to capture a wide range of leaf variations by sampling two age classes, replicates of species, and seasons. However, this study was focused on only three California ecosystems and is not representative of the total variation that would be captured

by HyspIRI. Lastly, our study used the AVIRIS and MASTER sensors to simulate the full spectrum from an airborne sensor perspective. The MASTER sensor has 25 channels for the TIR region, while the proposed HyspIRI satellite only has 8 channels (Green et al., 2013). Further analysis is needed using aerial imagery spectroscopy from the HyspIRI preparatory flight campaign to determine if this further spectral reduction would negatively affect vegetation biochemistry predictions. While there are challenges to overcome before using full spectrum spectroscopy on a global scale, this study does present a foundation for understanding how the full spectrum can improve prediction of vegetation properties using airborne and satellite sensors.

V. Conclusions

The first goal of this study was to use VSWIR and TIR spectra alone and combined to create PLSR models based on all samples, seasons, and plant functional types in order to evaluate each spectrum's ability to predict lignin, cellulose, nitrogen, water content, and LMA. The top performing model for each component using laboratory spectra showed high precision ($R^2 > 0.9$) and high accuracy (RMSE < 6.5%). These models for all biochemical and biophysical components used either the TIR or full spectrum and identified known absorption features. As seen in model results, the combination of VSWIR and TIR increased the R^2 value of regression models compared to VSWIR alone, signifying that the inclusion of TIR data would improve predictions of foliar chemistry and physiology.

The second goal was evaluating how these predictive relationships might change seasonally and among plant functional types. We found that model precision varied by season as well as across plant functional types, though the amount of variation depended on the analyzed component. Models developed for all samples generally resulted in decreased

R^2 values or required twice the number of factors compared to a single season or plant functional type. While AS model accuracy and precision was lower than seasonal or plant functional type models, these models are still appropriate to use for prediction of cellulose, nitrogen, and water content due to high model precision ($R^2 > 0.85$) and accuracy (RMSE < 7%). Models predicting foliar lignin content and LMA performed best when samples were divided into seasons or plant functional types.

To evaluate whether these relationships between spectra and foliar chemistry could be extended to the reduced spectral resolution available in airborne and proposed spaceborne sensors, we created PLSR models using AVIRIS, HyTES, and AVIRIS + MASTER simulated spectra. The models created from these spectra had reduced precision and accuracy compared to laboratory spectra. However, the top performing model for each component still had a high precision ($R^2 > 0.9$) and high accuracy (RMSE < 8%). When using simulated sensor spectra to predict biochemical contents, AVIRIS + MASTER produced the highest performing models, followed by HyTES. Similar to results using the laboratory spectra, the full spectrum as expressed using the AVIRIS + MASTER sensors increased the R^2 value of regression models compared to AVIRIS alone for the majority of models, signifying that the inclusion of TIR spectrum would improve predictions of vegetation properties.

In summary these results indicate that the TIR spectrum could augment the VSWIR in advancing identification of leaf biochemical and physical properties. Advancing this research beyond the leaf level will help determine if the full spectrum can outperform the VSWIR in predicting vegetation properties. The results we have seen using leaf level spectroscopy help set the foundation for the future use of full spectrum aerial and satellite imagery from instruments such as AVIRIS/MASTER and HyspIRI. This will expand the

possibilities for using full spectrum spectroscopy to quantify and characterize the world's ecosystems.

References

Arnold, S. L., & Schepers, J. S. (2004). A simple roller-mill grinding procedure for plant and soil samples. *Communications in Soil Science and Plant Analysis*, 35(3-4), 537–545.

Asner, G., & Martin, R. (2008). Spectral and chemical analysis of tropical forests: Scaling from leaf to canopy levels. *Remote Sensing of Environment*, 112(10), 3958–3970.

Asner, G. P., Martin, R. E., Ford, A. J., Metcalfe, D. J., & Liddell, M. J. (2009). Leaf chemical and spectral diversity in Australian tropical forests. *Ecological Applications*, 19(1), 236–53.

Asner, G. P., Martin, R. E., Knapp, D. E., Tupayachi, R., Anderson, C., Carranza, L., Martinez, P., Houcheime, M., Sinca, F., & Weiss, P. (2011). Spectroscopy of canopy chemicals in humid tropical forests. *Remote Sensing of Environment*, 115(12), 3587–3598.

Bolster, K. L., Martin, M. E., & Aber, J. D. (1996). Determination of carbon fraction and nitrogen concentration in tree foliage by near infrared reflectance: A comparison of statistical methods. *Canadian Journal of Forest Research*, 26, 590–600.

Boot, C.M., Schaeffer, S.M., & Schimel, J.P. (2013). Static osmolyte concentrations in microbial biomass during seasonal drought in a California grassland. *Soil Biology and Biochemistry*, 57, 356–361.

Burns, D.A. & Ciurczak, E.W. (2008). *Handbook of near-infrared analysis.*

Curran, P. J. (1989). Remote sensing of foliar chemistry. *Remote Sensing of Environment*, 30(3), 271–278.

Curran, P. J., Dungan, J. L., & Peterson, D. L. (2001). Estimating the foliar biochemical concentration of leaves with reflectance spectrometry: Testing the Kokaly and Clark methodologies. *Remote Sensing of Environment*, 76, 349–359.

Dahlgren, R.A., Boettinger, J.L., Huntington, G.L., & Amundson, R.G. (1997). Soil development along an elevational transect in the western Sierra Nevada, California. *Geoderma*, *78*, 207–236.

Da Silva Dias, R., De Abreu, C. A., De Abreu, M. F., Paz-Ferreiro, J., Matsura, E.E., & Paz González, A. (2013). Comparison of methods to quantify organic carbon in soil samples from São Paulo State, Brazil. *Communications in Soil Science and Plant Analysis*, 44(1-4), 429–439.

Doughty, C. E., Asner, G. P., & Martin, R. E. (2011). Predicting tropical plant physiology from leaf and canopy spectroscopy. *Oecologia*, 165(2), 289–99.

Dury, S. J., & Turner, B. J. (2001). Nutrient estimation of eucalypt foliage derived from hyperspectral data. *IEEE International Geoscience and Remote Sensing Symposium*, 2, 774–776.

Elvidge, C. D. (1988). Thermal infrared reflectance of dry plant materials: 2.5 – 20.0 μm. *Remote Sensing of Environment*, 26, 265–285.

Fabre, S., Lesaignoux, A., Olioso, A., & Briottet, X. (2011). Influence of water content on spectral reflectance of leaves in the 3 – 15 μm domain. *IEEE Geoscience and Remote Sensing Letters*, 8(1), 143–147.

Feilhauer, H., Asner, G.P., Martin, R.E., & Schmidtlein, S. (2010). Brightness-normalized partial least squares regression for hyperspectral data. *Journal of Quantitative Spectroscopy and Radiative Transfer*, 111, 1947–1957.

Ferwerda, J. G., Skidmore, A. K., & Mutanga, O. (2005). Nitrogen detection with hyperspectral normalized ratio indices across multiple plant species. *International Journal of Remote Sensing*, 26(18), 4083–4095.

Gao, B.C., & Goetz, A.F.H. (1995). Retrieval of equivalent water thickness and information related to biochemical components of vegetation canopies from AVIRIS data. *Remote Sensing of Environment*, 52, 155–162.

Green, R. O., Eastwood, M. L., Sarture, C. M., Chrien, T. G., Aronsson, M., Chippendale, B. J., Faust, J.A.,Pavri, B.E., Chovit, C.J., Solis, M., Olah, M.R., & Williams, O. (1998). Imaging spectroscopy and the Airborne Visible / Infrared Imaging Spectrometer (AVIRIS). *Remote Sensing of Environment*, 65, 227–248.

Green. R.O., McCubbin, I., and Hook, S.J. (2013). HyspIRI preparatory airborne campaign. *Proceedings of HyspIRI Workshop 2013.* Pasadena, California, 16 October.

Haaland, D.M., & Thomas, E.V. (1988). Partial least-squares methods for spectral analyses. 1. Relation to other quantitative calibration methods and the extraction of qualitative information. *Analytical Chemistry*, 60(11), 1193–1202.

Hatfield, R., & Fukushima, R. S. (2005). Can lignin be accurately measured? *Crop Science*, 45(3), 832–839.

Hook, S. J., Myers, J. J., Thome, K. J., Fitzgerald, M., & Kahle, A. B. (2001). The MODIS / ASTER airborne simulator (MASTER) a new instrument for earth science studies. *Remote Sensing of Environment*, 76, 93–102.

Huang, Z., Turner, B. J., Dury, S. J., Wallis, I.R., & Foley, W. J. (2004). Estimating foliage nitrogen concentration from HYMAP data using continuum removal analysis. *Remote Sensing of Environment*, *93*(1-2), 18–29.

Kokaly, R.F., & Clark, R.N. (1999). Spectroscopic determination of leaf biochemistry using band-depth analysis of absorption features and stepwise multiple linear regression. *Remote Sensing of Environment*, 67, 267–287.

Lawler, I.R., Aragones, L., Berding, N., Marsh, H., & Foley, W. (2006). Near-infrared reflectance spectroscopy is a rapid, cost-effective predictor of seagrass nutrients. *Journal of Chemical Ecology*, 32(6), 1353–65.

Martens, H., Karstang, T., & Naes, T. (1987). Improved selectivity in spectroscopy by multivariate calibration. *Journal of Chemometrics*, 1, 201–219.

Martin, M. E., & Aber, J. D. (1997). High spectral resolution remote sensing of forest canopy lignin, nitrogen, and ecosystem processes. *Ecological Applications*, 7(2), 431–443.

Martin, M.E., Plourde, L.C., Ollinger, S.V., Smith, M.L., & McNeil, B.E. (2008). A generalizable method for remote sensing of canopy nitrogen across a wide range of forest ecosystems. *Remote Sensing of Environment*, 112(9), 3511–3519.

Poorter, H., Niinemets, U., Poorter, L., Wright, I.J., & Villar, R. (2009). Causes and consequences of variation in leaf mass per area (LMA): A meta-analysis. *The New Phytologist*, 182(3), 565–88.

Quinn, R.D. and Keeley, S.C. (2006). Introduction to California chaparral. Los Angeles, California: University of California Press.

Ribeiro Da Luz, B. (2006). Attenuated total reflectance spectroscopy of plant leaves: a tool for ecological and botanical studies. *The New Phytologist*, 172(2), 305–18.

Ribeiro Da Luz, B., & Crowley, J. K. (2007). Spectral reflectance and emissivity features of broad leaf plants: Prospects for remote sensing in the thermal infrared (8.0 –14.0 μm). *Remote Sensing of Environment*, 109(4), 393–405.

Ribeiro Da Luz, B., & Crowley, J. K. (2010). Identification of plant species by using high spatial and spectral resolution thermal infrared (8.0 –13.5 μm) imagery. *Remote Sensing of Environment*, 114(2), 404–413.

Salisbury, J. W. (1986). Preliminary measurements of leaf spectral reflectance in the 8.0 – 14.0 μm region. *International Journal of Remote Sensing*, 7(12), 1879–1886.

Schneider, C.A, Rasband, W.S., & Eliceiri, K.W. (2012). NIH Image to ImageJ: 25 years of image analysis. *Nature Methods*, 9(7), 671–675.

Shenk, J.S., Westerhaus, M.O., & Hoover, M.R. (1979). Analysis of forages by infrared reflectance. *Journal of Dairy Science*, 62(5), 807–812.

Smith, M.L., Martin, M.E., Plourde, L., & Ollinger, S.V. (2003). Analysis of hyperspectral data for estimation of temperature forest canopy nitrogen concentration: Comparison between an airborne (AVIRIS) and a spaceborne (Hyperion) sensor. *IEEE Transactions on Geoscience and Remote Sensing*, 41(6), 1332– 1337.

Townsend, P.A., Foster, J.R., Chastain, R.A., & Currie, W.S. (2003). Application of imaging spectroscopy to mapping canopy nitrogen in the forests of the central Appalachian Mountains using Hyperion and AVIRIS. *IEEE Transactions on Geoscience and Remote Sensing*, 41(6), 1347–1354.

Ullah, S., Schlerf, M., Skidmore, A.K., & Hecker, C. (2012a). Identifying plant species using mid-wave infrared (2.5 – 6 μm) and thermal infrared (8 –14 μm) emissivity spectra. *Remote Sensing of Environment*, 118, 95–102.

Ullah, S., Skidmore, A. K., Naeem, M., & Schlerf, M. (2012b). An accurate retrieval of leaf water content from mid to thermal infrared spectra using continuous wavelet analysis. *Science of the Total Environment*, 437, 145–152.

Ullah, S., Skidmore, A.K., Groen, T. A., & Schlerf, M. (2013). Evaluation of three proposed indices for the retrieval of leaf water content from the mid-wave infrared (2-6 um) spectra. *Agricultural and Forest Meteorology*, 171-172, 65–71.

Ullah, S., Skidmore, A.K., Ramoelo, A., Groen, T.A., Naeem, M., & Ali, A. (2014). Retrieval of leaf water content spanning the visible to thermal infrared spectra. *ISPRS Journal of Photogrammetry and Remote Sensing*, 93, 56–64.

Ustin, S.L. (2013). Remote sensing of canopy chemistry. *Proceedings of the National Academy of Sciences of the United States of America*, 110(3), 804–5.

Wold, S., & Sjostrom, M. (2001). PLS-regression: a basic tool of chemometrics. *Chemometrics and Intelligent Laboratory Systems*, 58, 109–130.

Yoder, B.J., & Pettigrew-Crosby, R. E. (1995). Predicting nitrogen and chlorophyll content and concentrations from reflectance spectra (400 - 2500 nm) at leaf and canopy scales. *Remote Sensing of Environment*, 53, 199–211.

Young, S. J., Johnson, R., & Hackwell, J. A. (2002). An in-scene method for atmospheric compensation of thermal hyperspectral data. *Journal of Geophysical Research*, 107(D24), ACH 14–1 – ACH 14–20.

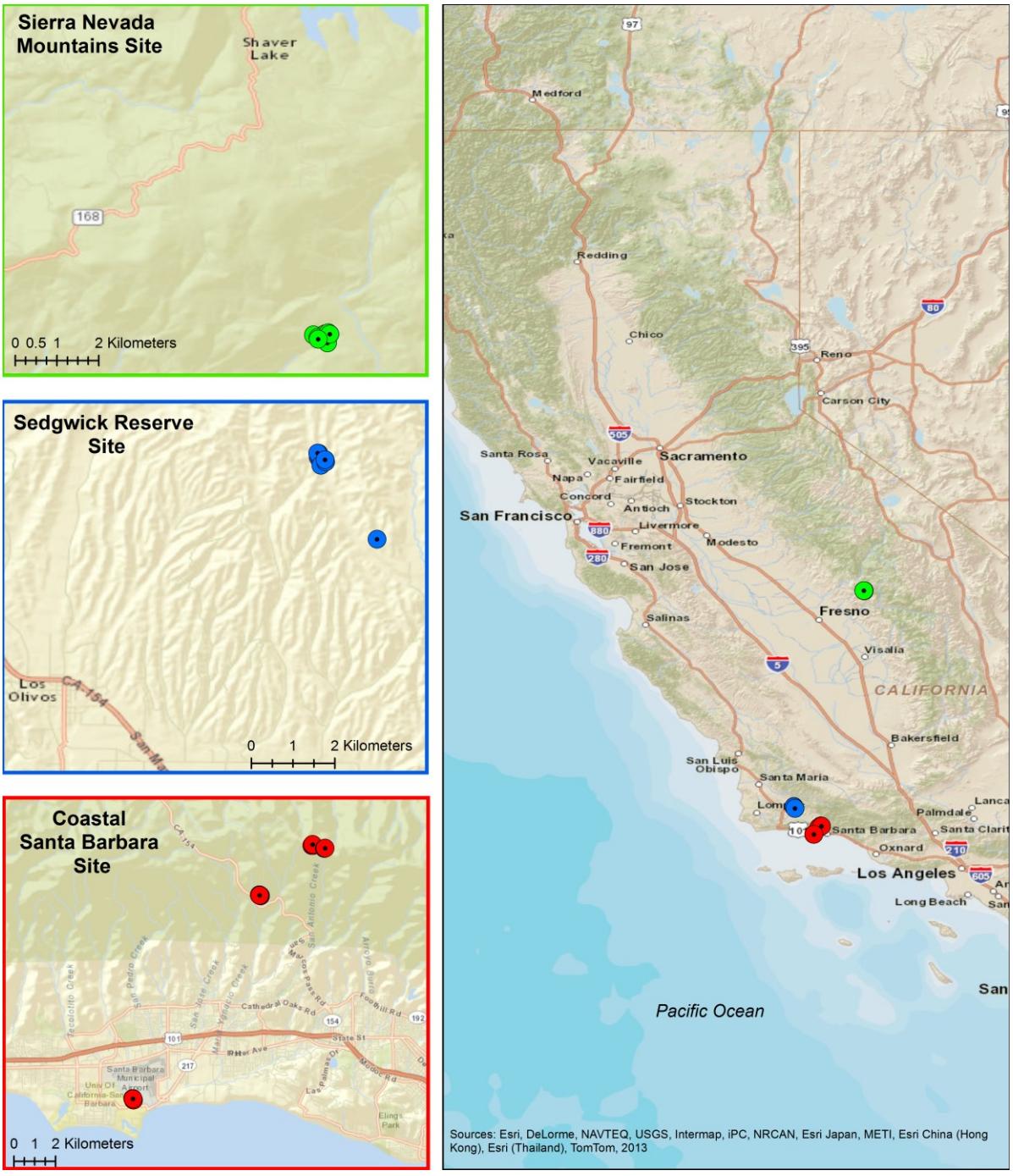

Figure 1. Map showing locations of study sites

Table 1. Species sampled in the study

Species	Common Name	Abb.	Site	Plant Functional Type	Sampling Dates
Abies concolor	White Fir	ABCO	Sierra Nevada	NE	April 20, June 8, Nov. 2
Adenostoma fasciculatum	Chamise	ADFA	Santa Barbara	NE	April 1, June 3, Oct. 13
Arctostaphylos glandulosa	Manzanita	ARGL	Santa Barbara	BE	April 1, June 3, Oct. 13
Baccharis pilularis	Coyote Brush	BAPI	Santa Barbara	BE	April 1, June 3, Oct. 13
Calocedrus decurrens	Incense Cedar	CADE	Sierra Nevada	NE	April 20, June 8, Nov. 2
Ceanothus cuneatus	Buck-brush Ceanothus	CECU	Santa Barbara	BE	April 1, June 3, Oct. 13
Ceanothus megacarpus	Big-pod Ceanothus	CEME	Santa Barbara	BE	April 1, June 3, Oct. 13
Ceanothus spinosus	Green-bark Ceanothus	CESP	Santa Barbara	BE	April 1, June 3, Oct. 13
Heteromeles arbutifolia	Toyon	HEAR	Santa Barbara	NE	April 1, June 3, Oct. 13
Pinus lambertiana	Sugar Pine	PILA	Sierra Nevada	NE	April 20, June 8, Nov. 2
Pinus ponderosa	Ponderosa Pine	PIPO	Sierra Nevada	NE	April 20, June 8, Nov. 2
Quercus agrifolia	Coast Live Oak	QUAG	Sedgwick Reserve	BE	April 21, June 9, Nov. 3
Quercus douglasii	Blue Oak	QUDO	Sedgwick Reserve	BD	April 21, June 9, Nov. 3
Quercus lobata	Valley Oak	QULO	Sedgwick Reserve	BD	April 21, June 9, Nov. 3
Salvia leucophylla	Purple Sage	SALE	Sedgwick Reserve	BD	April 21, June 9, Nov. 3
Umbellularia californica	Bay Laurel	UMCA	Santa Barbara	BE	April 1, June 3, Oct. 13

Note: Plant Functional Type is cateogorized by broadleaf deciduous (BD), broadleaf evergreen (BE), and needleleaf evergreen (NE).

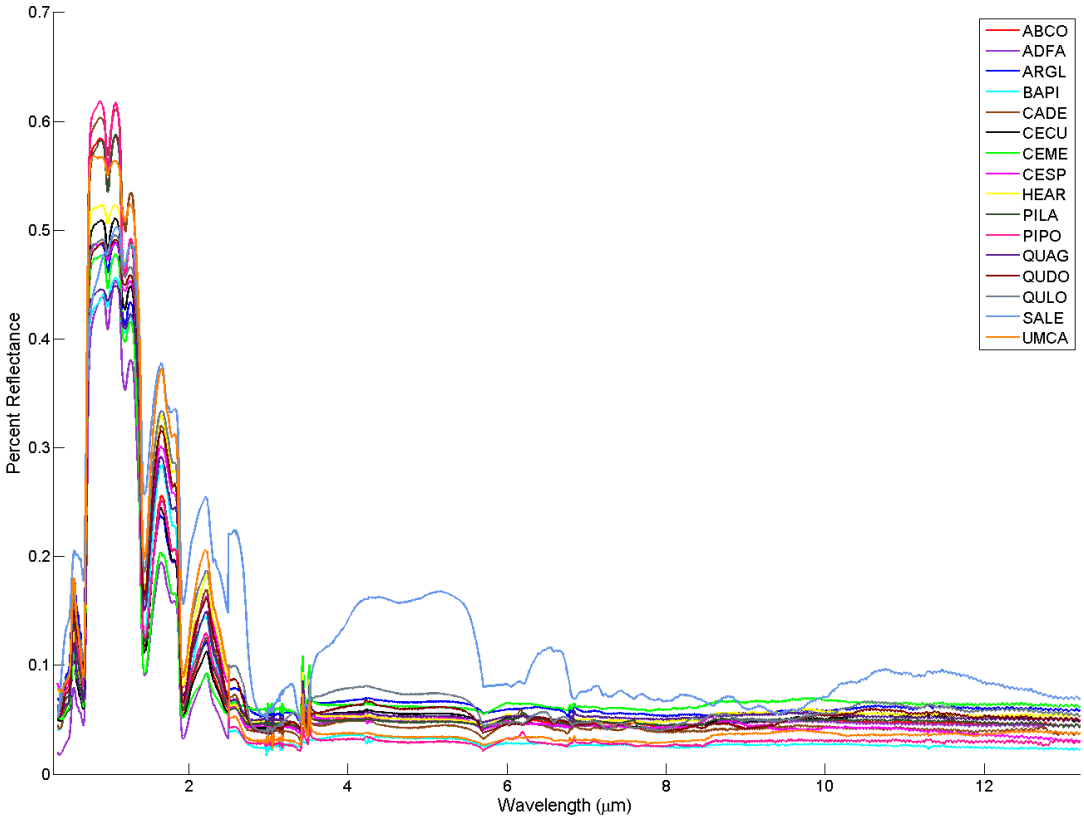

Figure 2. Mean spectra of sixteen vegetation species, each spectrum is the average of 18 samples measured.

Table 2. Foliar cellulose, lignin, nitrogen, water, and LMA results for the sixteen target species averaged for all seasons and leaf ages.

	Sample	Cellulose (%)				Lignin (%)				Nitrogen (%)				Water Content (%)				LMA (g/m^2)			
	Size	Mean	Min	Max	SD	Mean	Min	Max	SD	Mean	Min	Max	SD	Mean	Min	Max	SD	Mean	Min	Max	SD
ABCO	18	13.4	10.7	16.9	1.7	10.8	8.6	13.0	1.3	0.91	0.74	1.20	0.12	53.5	46.5	60.8	4.3	3.13	2.45	3.76	0.41
ADFA	18	10.3	8.1	17.4	2.7	12.3	10.3	15.0	1.2	1.18	0.48	2.28	0.42	49.4	36.1	74.1	10.1	4.22	1.73	6.80	1.23
ARGL	18	6.8	5.5	8.1	0.7	10.9	8.0	14.6	1.8	0.72	0.45	1.07	0.16	47.0	40.2	61.7	6.7	2.66	1.29	4.73	0.93
BAPI	18	9.8	6.9	13.3	1.9	11.9	7.4	16.3	3.0	2.49	0.96	3.60	0.64	68.6	55.0	76.9	6.4	0.66	0.40	1.01	0.16
CADE	18	13.1	10.4	16.9	1.7	12.5	10.6	14.8	1.3	0.96	0.72	1.45	0.20	50.2	44.7	56.1	3.9	2.89	1.42	4.68	0.90
CECU	18	9.2	5.9	13.1	1.9	13.1	5.7	22.5	5.7	1.70	0.98	3.39	0.59	50.8	41.7	69.2	6.8	2.38	1.30	5.39	1.19
CEME	18	5.9	4.5	8.4	1.0	5.6	4.1	6.9	0.8	1.30	0.91	1.95	0.28	46.0	35.8	58.7	8.0	2.69	2.27	3.25	0.27
CESP	18	5.2	4.2	6.4	0.6	3.3	2.6	5.5	0.7	1.66	1.35	2.00	0.17	50.1	41.0	60.5	6.1	1.06	0.68	1.43	0.22
HEAR	18	10.4	8.5	14.0	1.6	10.2	7.0	12.0	1.1	1.31	0.78	2.02	0.29	53.5	47.4	66.6	5.0	1.69	0.60	2.53	0.46
PILA	18	18.2	16.0	20.9	1.5	10.1	8.7	11.9	1.0	0.90	0.69	1.40	0.17	52.2	44.2	58.8	4.5	3.26	2.21	4.53	0.74
PIPO	18	21.9	16.8	27.3	2.7	12.7	10.4	16.5	1.5	1.08	0.68	1.65	0.22	53.7	34.0	71.8	9.6	5.01	1.56	7.13	1.67
QUAG	18	18.7	14.9	21.6	1.5	12.1	10.0	14.0	1.3	1.30	0.79	2.19	0.29	43.6	28.8	61.5	5.8	2.40	1.14	3.41	0.57
QUDO	18	13.5	10.3	16.1	1.7	6.6	4.7	9.3	1.1	1.92	0.80	2.45	0.50	49.7	29.8	62.0	8.1	1.29	0.82	2.95	0.54
QULO	18	12.7	11.4	14.2	0.7	8.9	7.1	11.1	1.2	1.75	0.82	2.41	0.46	52.0	38.0	62.4	6.0	1.20	0.79	2.11	0.31
SALE	18	9.7	7.7	12.0	1.3	11.9	9.0	14.5	1.4	1.80	0.80	2.42	0.43	38.9	20.2	56.1	13.1	1.91	0.86	3.35	0.78
UMCA	18	10.0	7.5	11.5	1.2	11.8	10.4	15.6	1.4	2.16	1.06	3.81	0.78	54.1	46.9	75.3	9.1	1.14	0.46	2.52	0.49

Table 3. Results of one-way ANOVA for seasonal foliage collections.

Species	Lignin	Cellulose	Nitrogen	Water Content	LMA
ABCO	0.613	0.441	0.766	0.002**	0.174
ADFA	0.054	0.015*	0.006**	0.000**	0.998
ARGL	0.825	0.598	0.201	0.004**	0.624
BAPI	0.000**	0.030*	0.000**	0.000**	0.009**
CADE	0.000**	0.139	0.915	0.100	0.048*
CECU	0.000**	0.002**	0.129	0.011*	0.003**
CEME	0.937	0.157	0.020*	0.000**	0.007**
CESP	0.028*	0.931	0.308	0.000**	0.675
HEAR	0.004**	0.798	0.600	0.018*	0.252
PILA	0.000**	0.027*	0.837	0.004**	0.090
PIPO	0.008**	0.042*	0.040*	0.385	0.048*
QUAG	0.389	0.710	0.590	0.121	0.038*
QUDO	0.748	0.991	0.000**	0.000**	0.038*
QULO	0.032*	0.672	0.002**	0.000**	0.059
SALE	0.205	0.983	0.002**	0.000**	0.003**
UMCA	0.053	0.031*	0.213	0.008**	0.638

Note: Values reported are p-values that represent the level at which significant differences occurred among the three seasons. One asterisk (*) indicates $p < 0.05$ and two asterisks (**) indicate $p < 0.01$.

Table 4. Statistics for partial least squares regressions (PLSR) including top performing laboratory spectra for each model category.

Model Description	Lignin				Cellulose				Nitrogen				Moisture Content				LMA			
	Spectrum	R^2	Factors	% RMSE	Spectrum	R^2	Factors	% RMSE	Spectrum	R^2	Factors	% RMSE	Spectrum	R^2	Factors	% RMSE	Spectrum	R^2	Factors	% RMSE
All Samples	Full	0.62	11	6.20	VSWIR	0.95	34	4.64	VSWIR	0.88	25	6.20	Full	0.92	13	4.59	Full	0.78	12	8.67
Spring Season	Full	0.83	11	9.12	Full	0.93	16	6.04	Full	0.93	12	6.61	TIR	0.97	13	3.26	VSWIR	0.83	7	9.14
Summer Season	TIR	0.89	10	6.54	TIR	0.97	12	4.22	TIR	0.85	7	7.71	Full	0.91	10	6.30	TIR	0.89	9	6.36
Fall Season	TIR	0.82	7	7.40	VSWIR	0.89	15	7.00	TIR	0.90	8	7.43	TIR	0.92	8	5.01	TIR	0.98	10	3.03
Broadleaf Deciduous	Full	0.93	10	6.42	Full	0.76	8	10.71	Full	0.96	11	5.38	TIR	0.97	7	4.18	TIR	0.88	6	8.13
Broadleaf Evergreen	VSWIR	0.91	23	6.11	Full	0.94	17	5.46	VSWIR	0.81	14	7.76	Full	0.92	7	5.75	TIR	0.88	12	6.46
Needleleaf Evergreen	Full	0.76	11	8.81	VSWIR	0.96	19	6.27	TIR	0.89	8	4.70	TIR	0.92	6	4.77	Full	0.76	10	9.95

Table 5. Statistics for partial least squares regressions (PLSR) including top performing sensor simulated spectra for each model category.

Model Description	Lignin				Cellulose				Nitrogen				Moisture Content				LMA			
	Spectrum	R^2	Factors	% RMSE	Spectrum	R^2	Factors	% RMSE	Spectrum	R^2	Factors	% RMSE	Spectrum	R^2	Factors	% RMSE	Spectrum	R^2	Factors	% RMSE
All Samples	HyTES	0.59	8	8.17	AVIRIS	0.93	33	7.78	AVIRIS	0.86	26	7.82	AVIRIS+ MASTER	0.93	19	4.23	AVIRIS+ MASTER	0.75	12	9.06
Spring Season	HyTES	0.93	10	6.23	HyTES	0.86	9	8.96	AVIRIS+ MASTER	0.89	11	7.36	AVIRIS	0.89	9	7.24	AVIRIS+ MASTER	0.82	8	9.41
Summer Season	HyTES	0.87	9	8.25	AVIRIS+ MASTER	0.95	22	5.00	AVIRIS	0.71	10	8.71	AVIRIS+ MASTER	0.89	7	6.86	AVIRIS+ MASTER	0.84	10	7.52
Fall Season	HyTES	0.80	8	7.68	AVIRIS+ MASTER	0.90	15	7.01	AVIRIS+ MASTER	0.56	5	11.85	AVIRIS+ MASTER	0.88	8	6.22	AVIRIS	0.74	7	8.91
Broadleaf Deciduous	AVIRIS+ MASTER	0.92	10	6.97	HyTES	0.77	6	10.03	HyTES	0.92	9	7.59	HyTES	0.99	11	2.68	HyTES	0.98	11	3.15
Broadleaf Evergreen	HyTES	0.79	8	8.52	AVIRIS+ MASTER	0.89	16	7.59	AVIRIS+ MASTER	0.81	16	8.07	AVIRIS+ MASTER	0.89	7	6.29	AVIRIS+ MASTER	0.80	10	7.90
Needleleaf Evergreen	HyTES	0.80	6	8.42	AVIRIS	0.98	26	3.32	HyTES	0.82	6	5.86	AVIRIS+ MASTER	0.87	9	6.28	HyTES	0.66	4	10.43

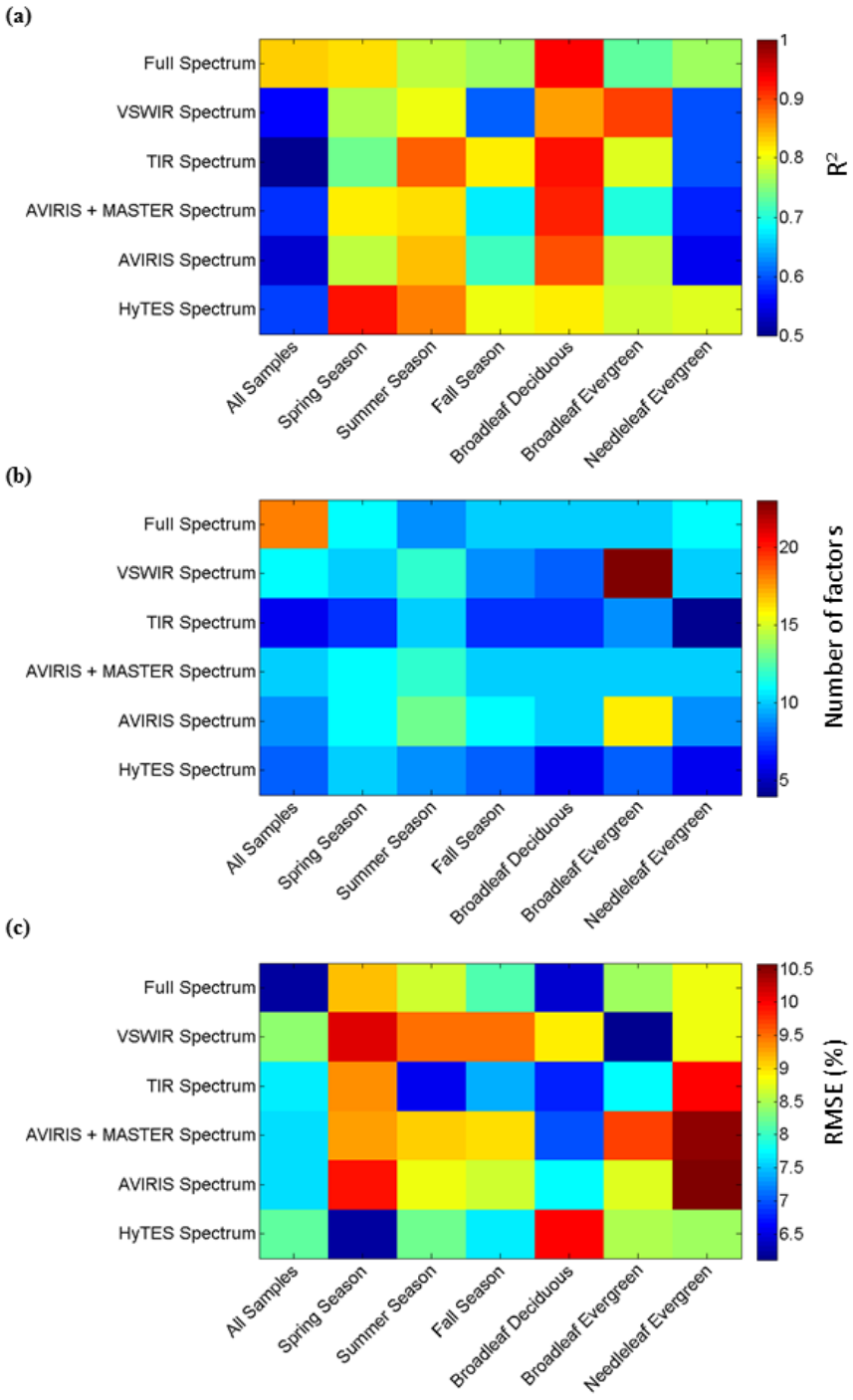

Figure 3. Visual representation of model results predicting lignin with (a) R^2, (b) number of factors, and (c) % RMSE used in each model.

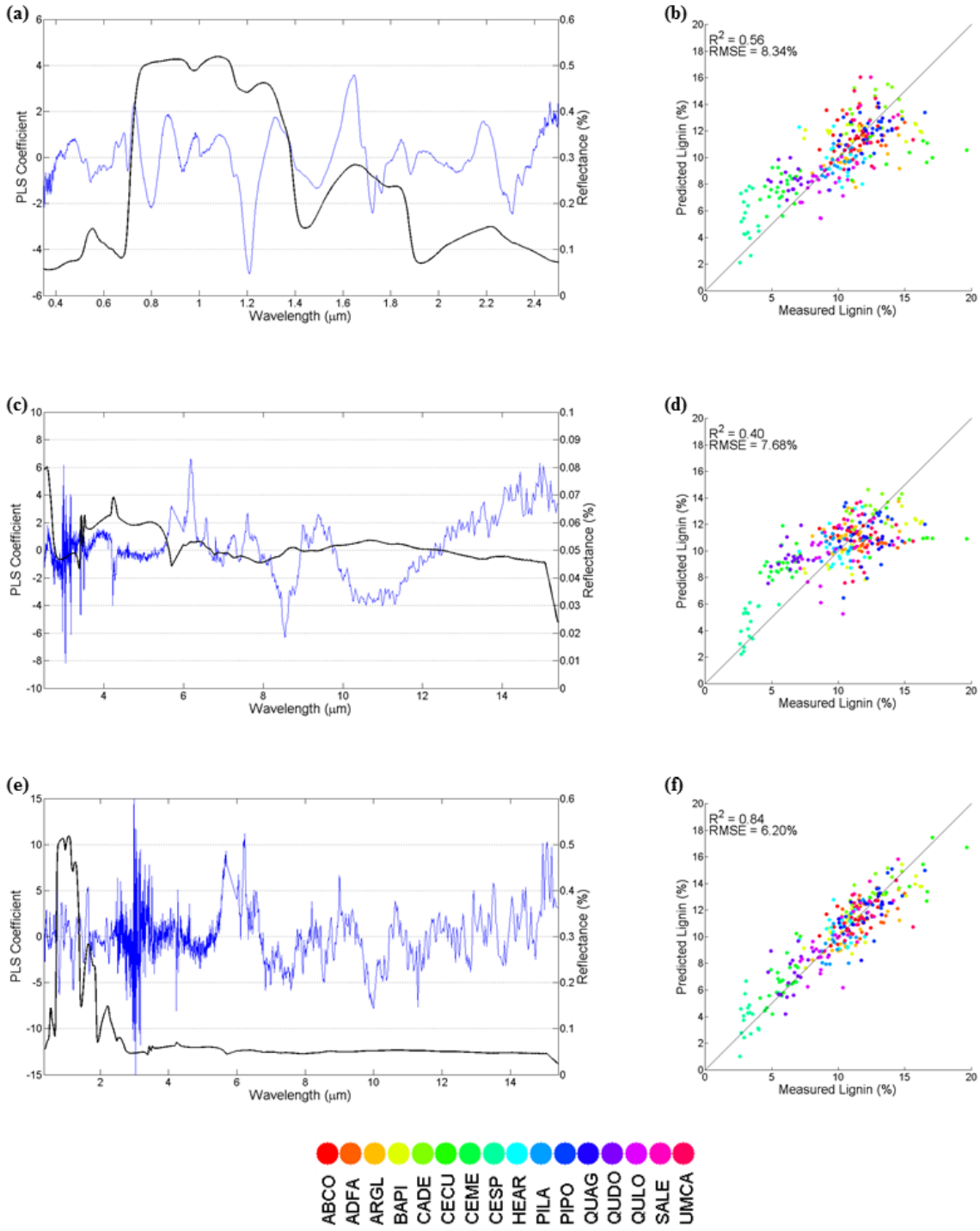

Figure 4. The PLSR coefficients (blue line) showing the importance of each wavelength in developing the PLSR model for retrieving lignin content from the (a) VSWIR, (c) TIR, and (e) full spectrum. The average reflectance spectrum (black line) is shown for reference purpose. Predicted versus laboratory measured lignin content is shown using the (b) VSWIR, (d) TIR, and (f) full spectrum.

Table 6. PLSR model created from all samples for lignin, cellulose, nitrogen, water content, and LMA with wavelength (µm) and corresponding chemical structure. Data shown are wavelengths that had the top four largest PLSR coefficients listed from largest to smallest magnitude.

	Full Spectrum		VSWIR Spectrum		TIR Spectrum	
Lignin	6.21	Lignin	1.21	$.CH_2$ *	6.19	Lignin
	5.70	Lignin	1.65	Lignin^	8.56	Wax
	2.99	Lignin, Cellulose	2.50	Starch *	14.21	Cellulose
	9.95	Cellulose	2.31	Protein *	10.52	Wax
Cellulose	3.42	$.CH_2$	2.48	Cellulose*	14.21	Cellulose
	3.02	Cellulose	2.48	$.CH_2$, Protein*	3.42	$.CH_2$
	3.07	Cellulose	0.99	Starch^	2.96	Cellulose**
	11.47	Wax	1.23	$.CH_2$ *	15.03	Cellulose**
Nitrogen	3.16	Cellulose	2.49	Cellulose*	2.97	Lignin
	3.05	Cellulose	1.00	Starch^	3.02	Cellulose
	3.42	H-C Vibration Bands**	1.66	Nitrogen^	3.16	Cellulose
	5.67	Lignin	2.13	Protein^	13.00	Lignin
Water Content	3.16	Cellulose	1.00	Water^	2.97	Water**
	2.97	Water**	0.52	Chlorophyll b^	14.44	Water
	3.42	H-C Vibration Bands**	1.59	Starch^	3.17	Cellulose
	4.23	Lignin	2.04	Urea*	6.20	Water**
LMA	3.42	$.CH_2$, Cellulose	1.21	Water, Cellulose, Starch, Lignin^	6.20	Lignin
	2.99	Cellulose, Humic Acid	0.41	Chlorophyll A^	2.99	Cellulose, Humic Acid
	3.05	OH Stretching	1.41	Aromatic*	6.19	Water
	3.51	$.CH_2$, Cellulose	1.91	Starch^	11.87	Lignin

Note: Chemical structures are within 0.01 µm of specified wavelengths according to Elvidge (1988), except where marked with * (Burns and Ciurczak, 2008), ** (Fabre et al., 2011), and a ^ (Curran, 1989).

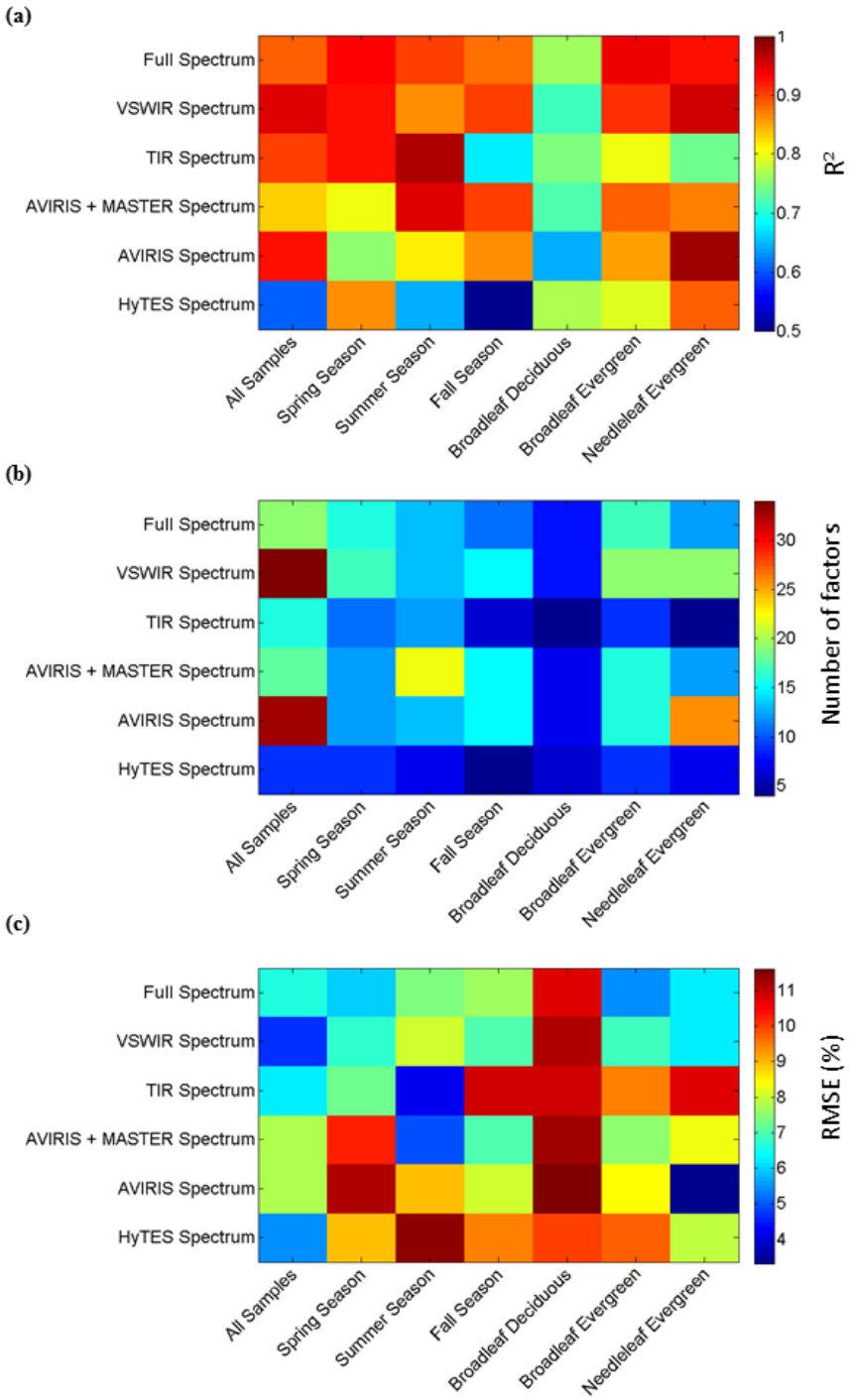

Figure 5. Visual representation of model results predicting cellulose with (a) R^2, (b) number of factors, and (c) % RMSE used in each model.

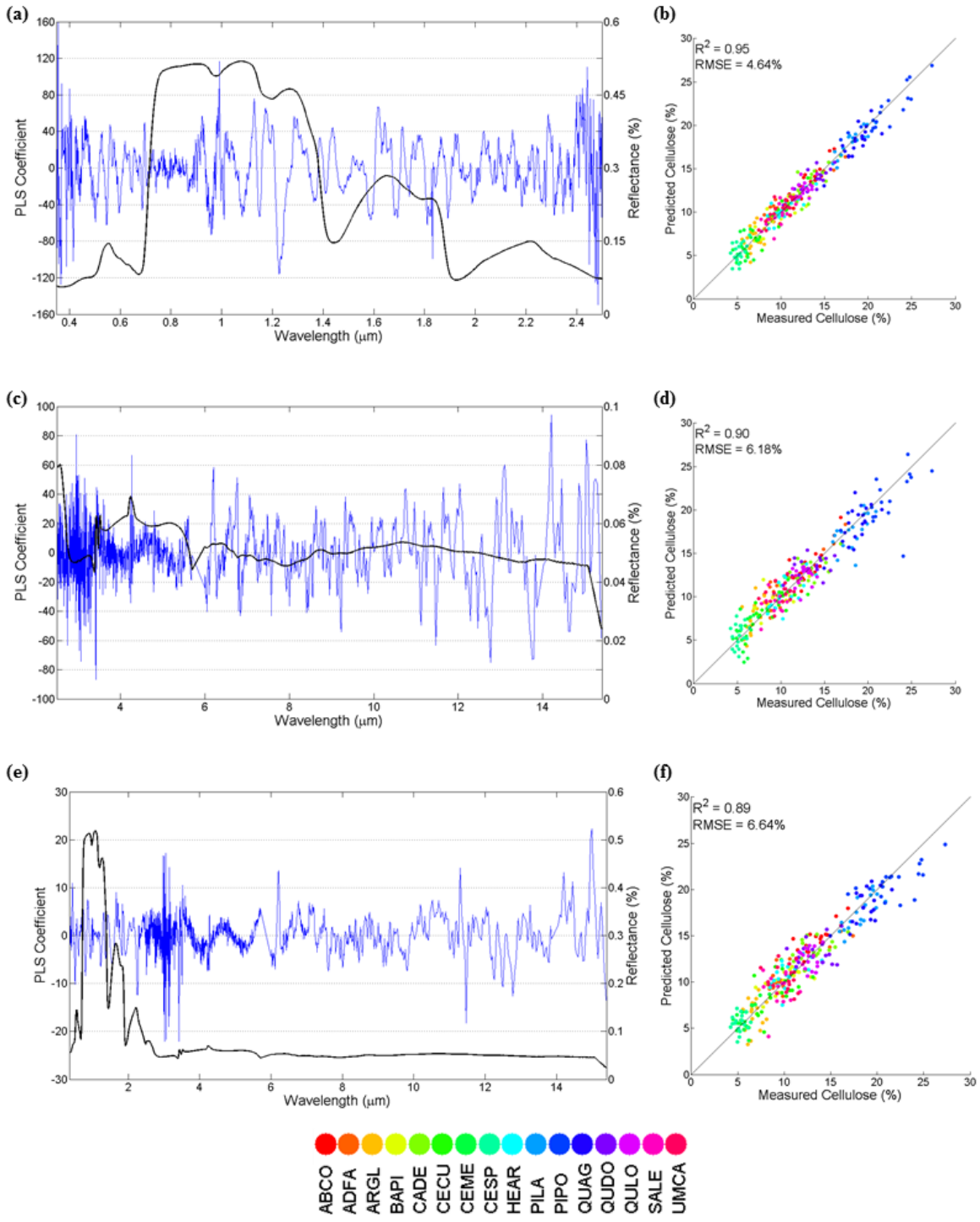

Figure 6. The PLSR coefficients (blue line) showing the importance of each wavelength in retrieving cellulose content using the (a) VSWIR, (c) TIR, and (e) full spectrum. The average reflectance spectrum (black line) is shown for reference purpose. Predicted versus laboratory measured cellulose content is shown using the (b) VSWIR, (d) TIR, and (f) full spectrum.

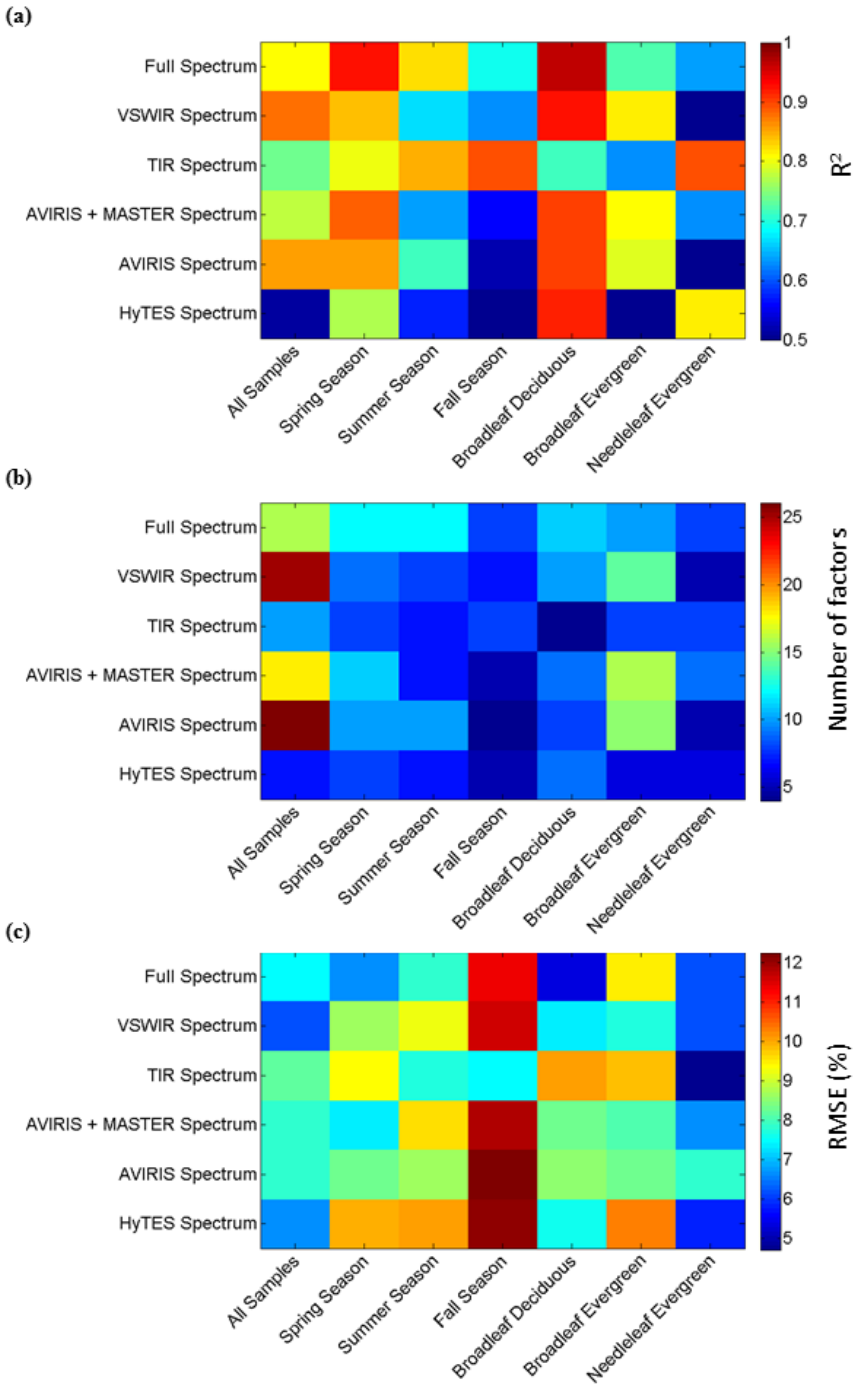

Figure 7. Visual representation of model results predicting nitrogen with (a) R^2, (b) number of factors, and (c) % RMSE used in each model.

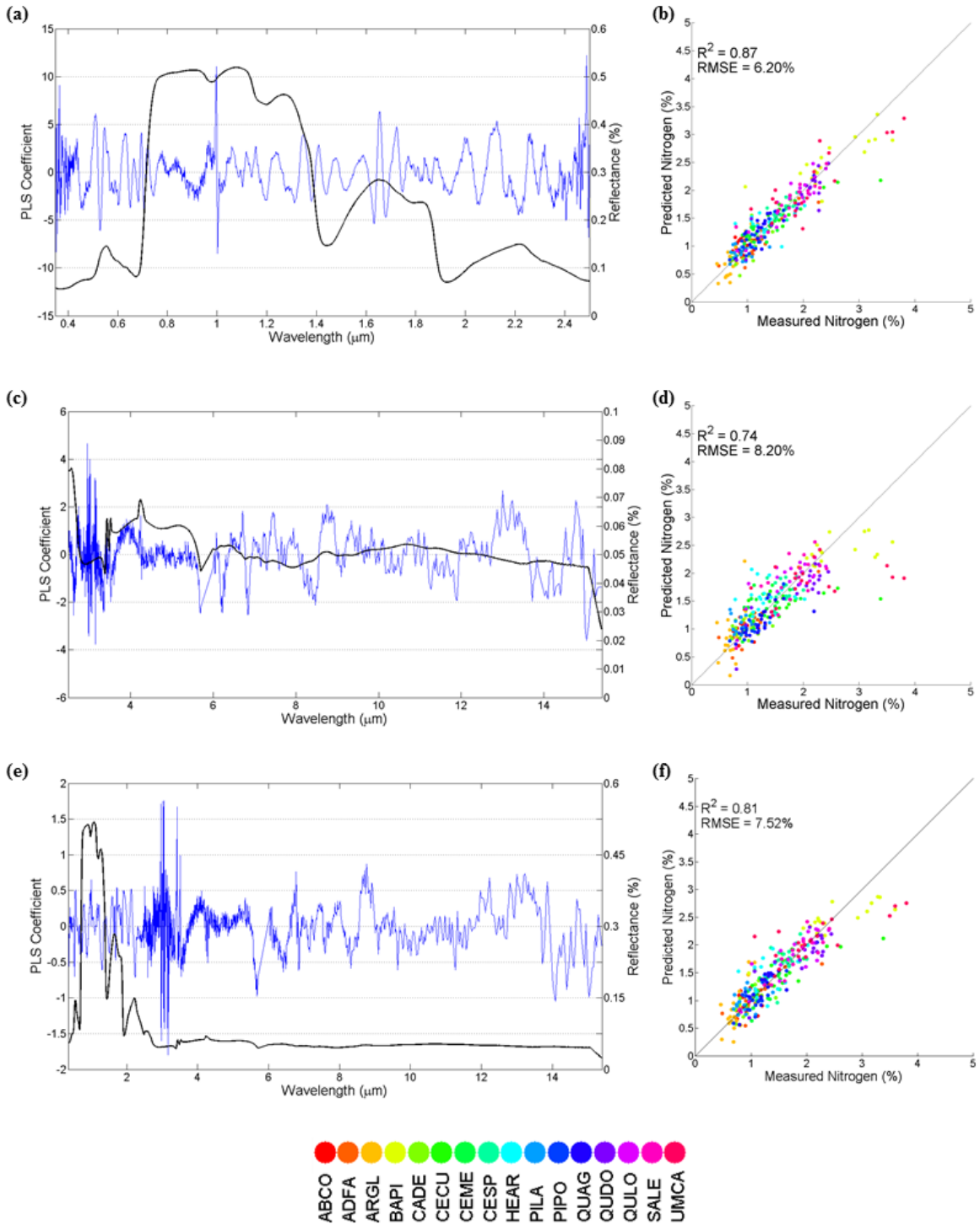

Figure 8. The PLSR coefficients (blue line) showing the importance of each wavelength in developing the PLSR model for retrieving nitrogen content from the (a) VSWIR, (c) TIR, and (e) full spectrum. The average reflectance spectrum (black line) is shown for reference purpose. Predicted versus laboratory measured nitrogen content is shown using the (b) VSWIR, (d) TIR, and (f) full spectrum.

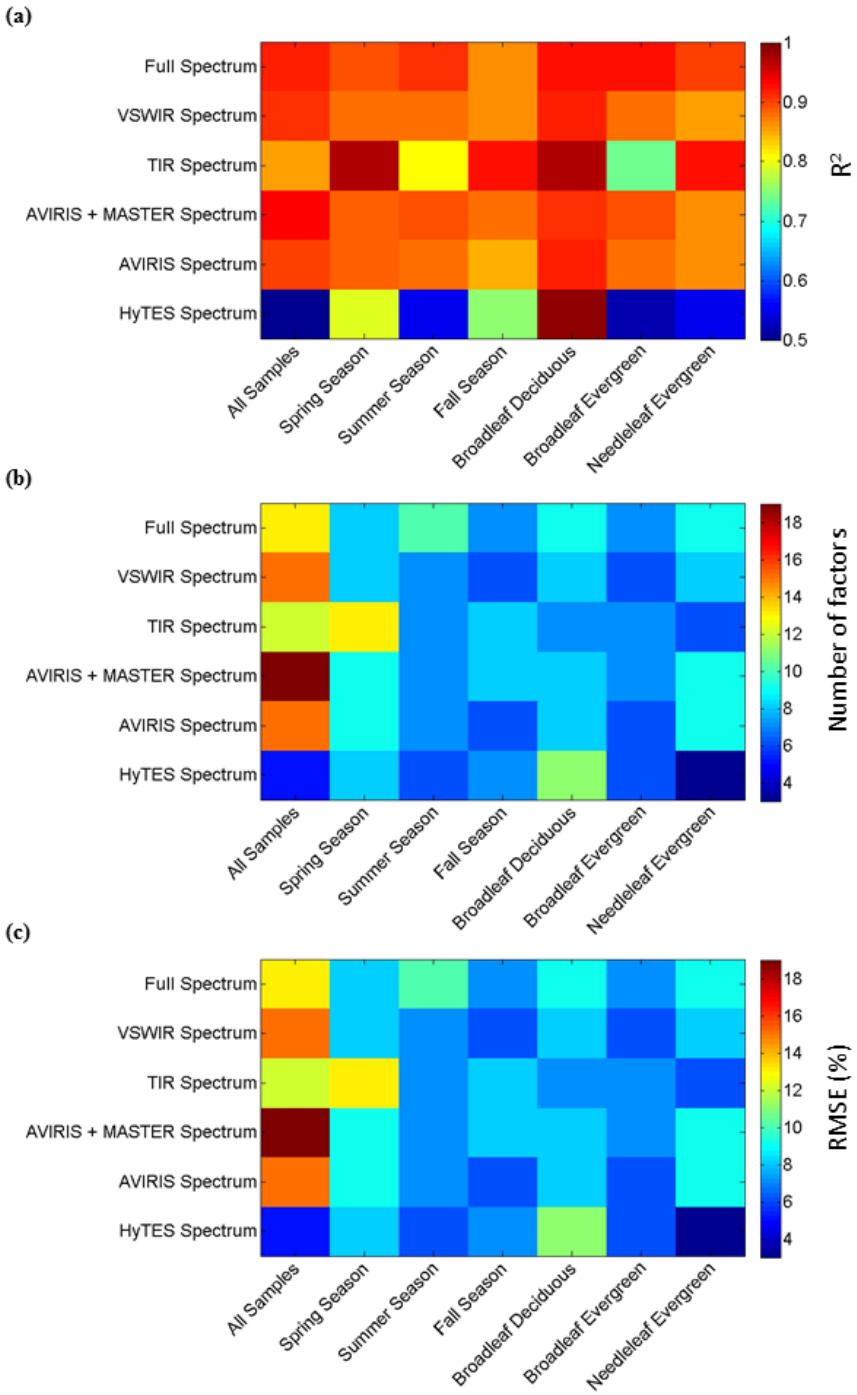

Figure 9. Visual representation of model results predicting water content with (a) R^2, (b) number of factors, and (c) % RMSE used in each model.

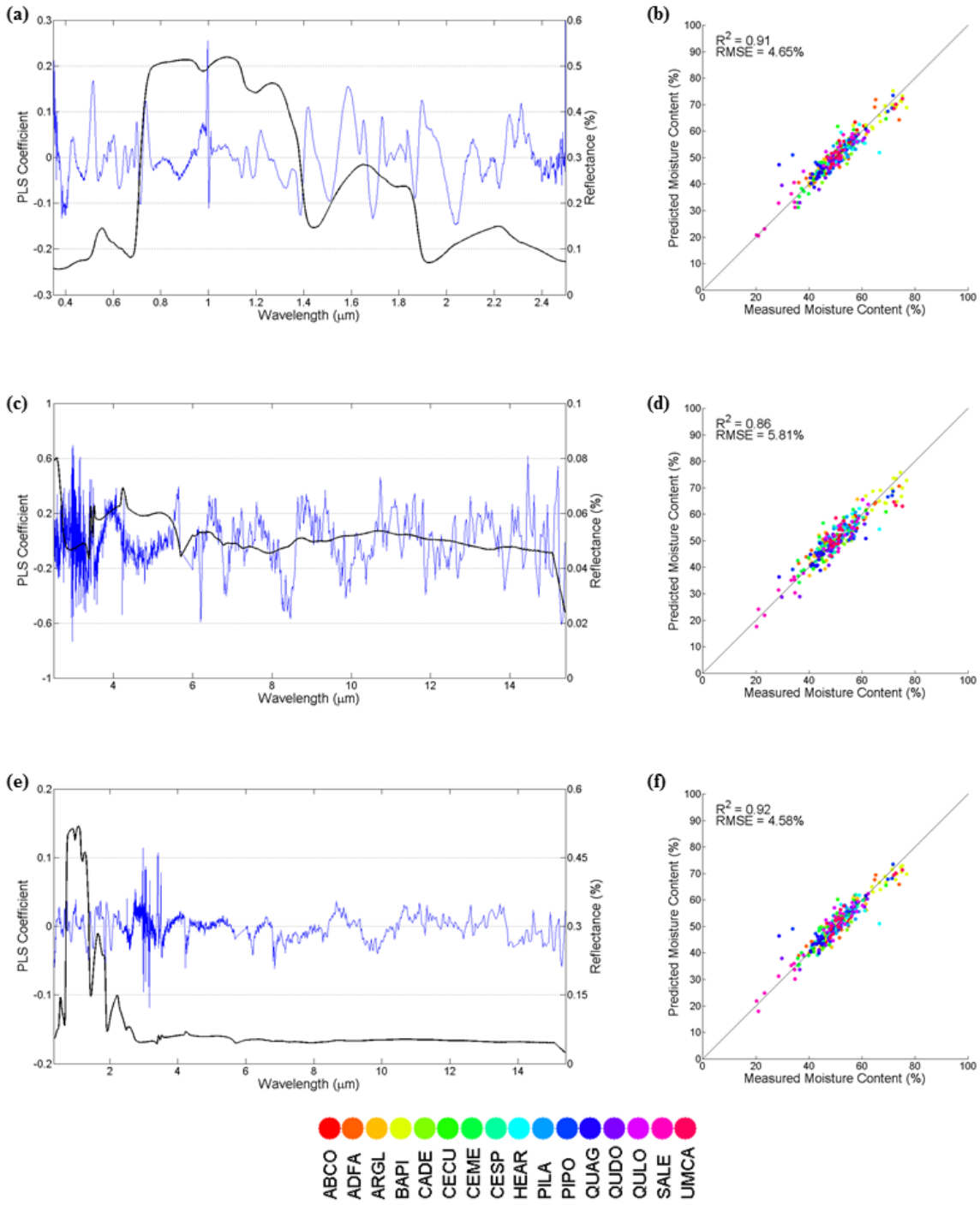

Figure 10. The PLSR coefficients (blue line) showing the importance of each wavelength in developing the PLSR model for retrieving water content from the (a) VSWIR, (c) TIR, and (e) full spectrum. The average reflectance spectrum (black line) is shown for reference purpose. Predicted versus laboratory measured water content is shown using the (b) VSWIR, (d) TIR, and (f) full spectrum.

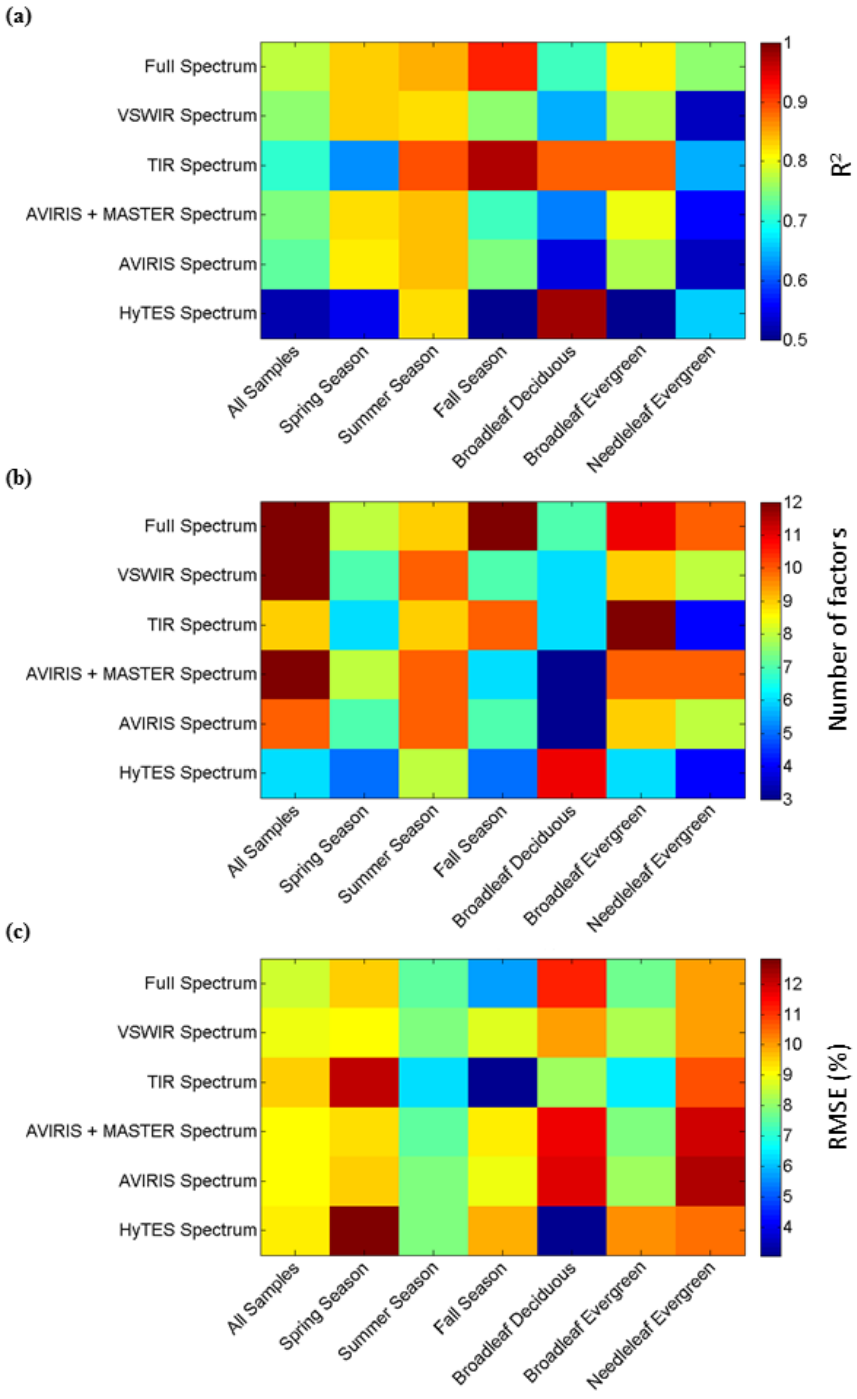

Figure 11. Visual representation of model results predicting LMA with (a) R^2, (b) number of factors, and (c) % RMSE used in each model.

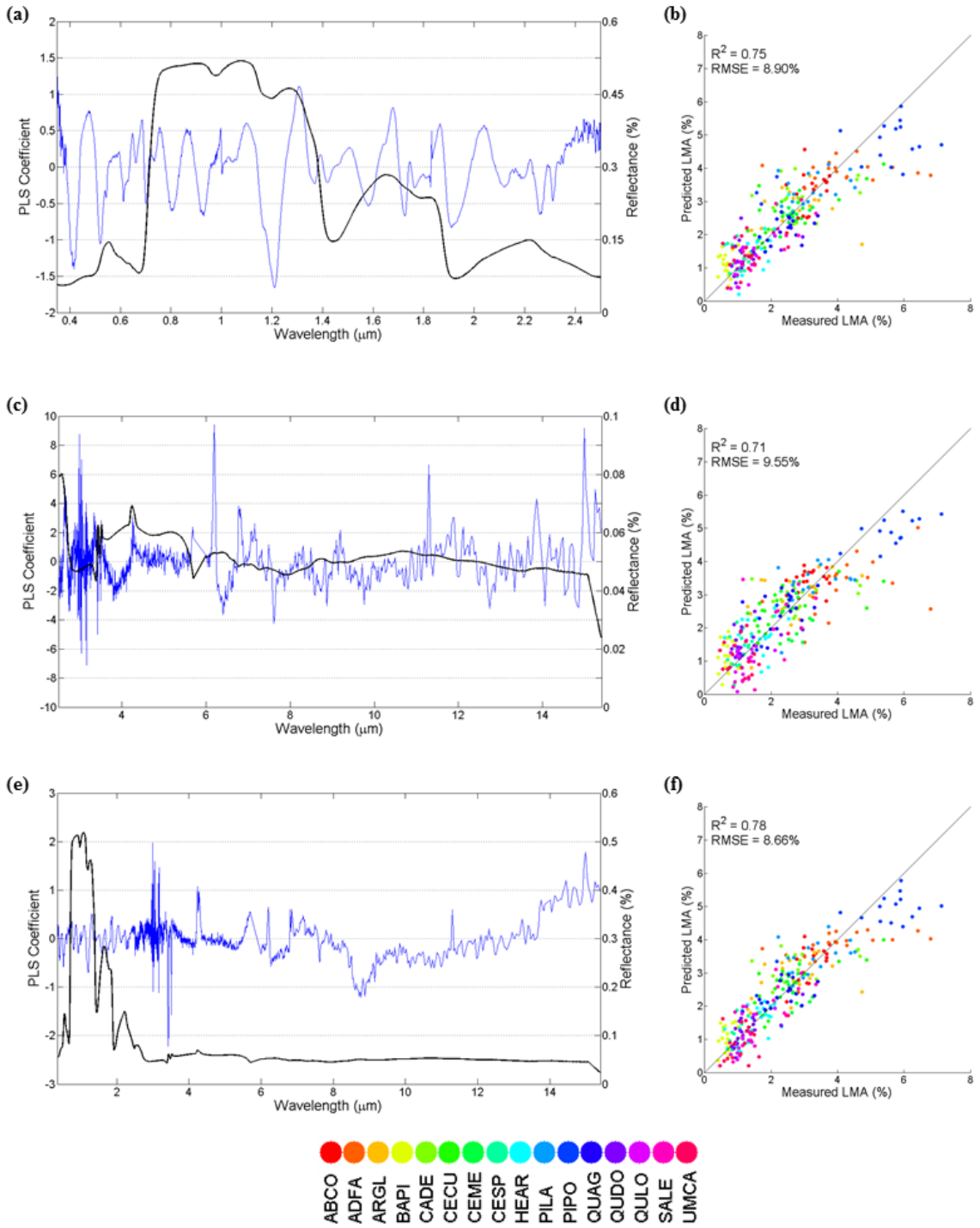

Figure 12. The PLSR coefficients (blue line) showing the importance of each wavelength in developing the PLSR model for retrieving LMA from the (a) VSWIR, (c) TIR, and (e) full spectrum. The average reflectance spectrum (black line) is shown for reference purpose. Predicted versus laboratory measured LMA is shown using the (b) VSWIR, (d) TIR, and (f) full spectrum.

Appendix

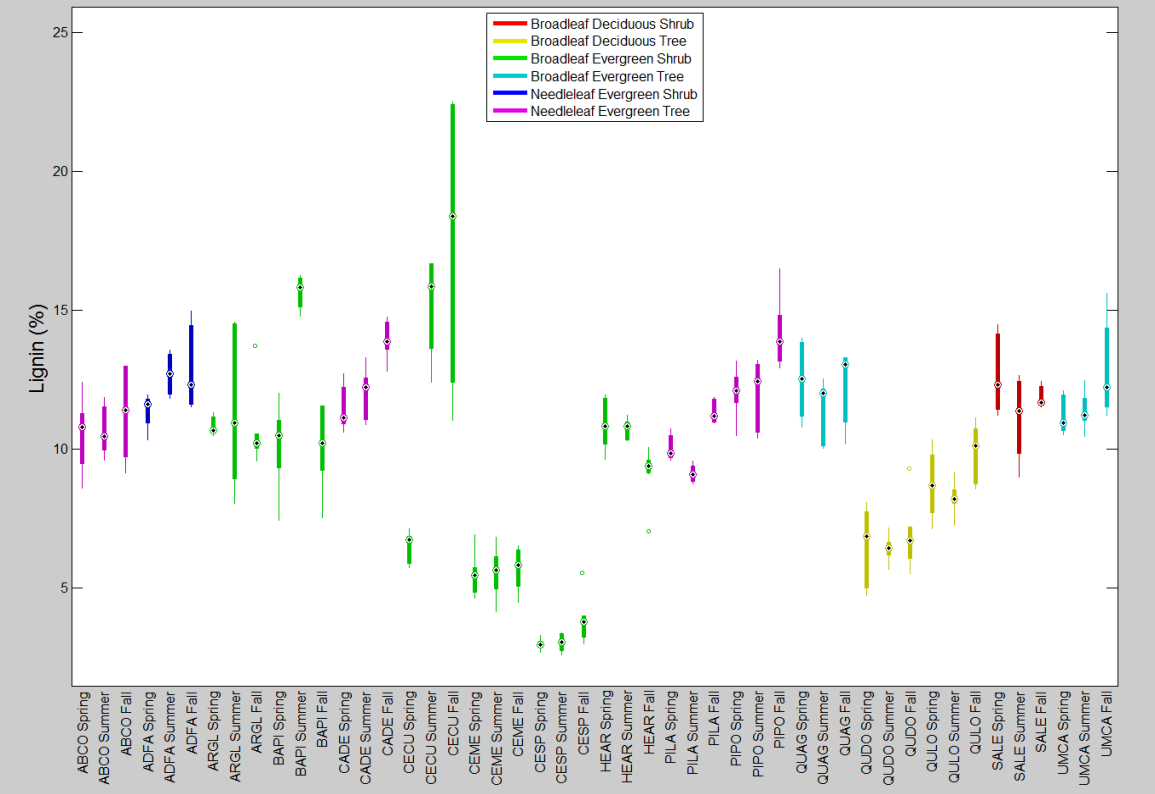

Figure A1. Seasonal distribution of lignin content for all species.

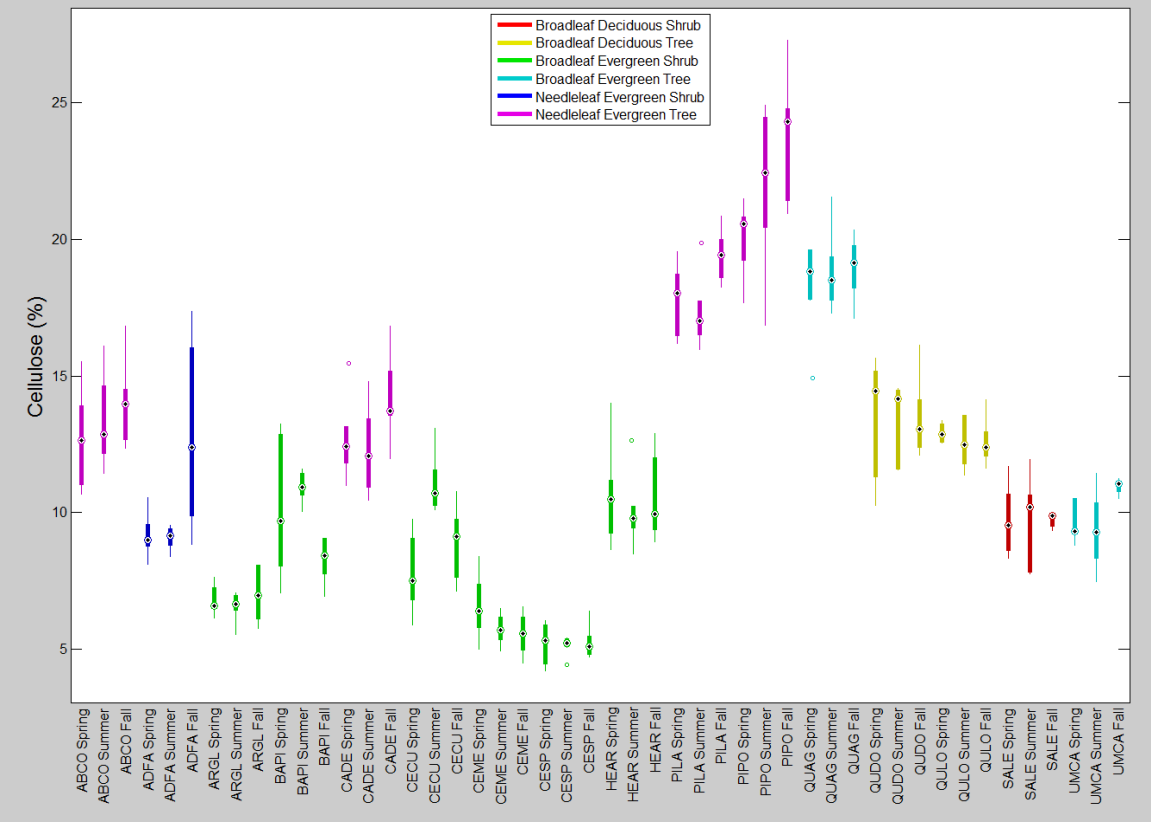

Figure A2. Seasonal distribution of cellulose content for all species.

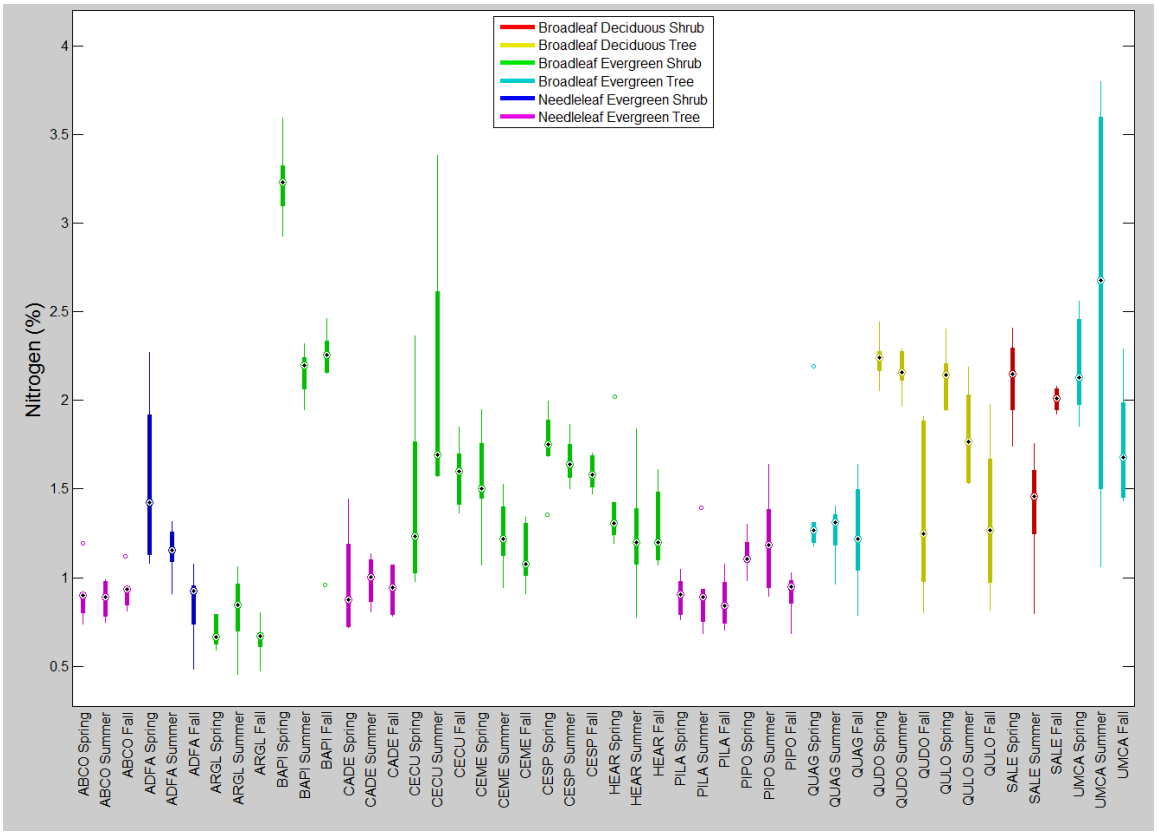

Figure A3. Seasonal distribution of nitrogen content for all species.

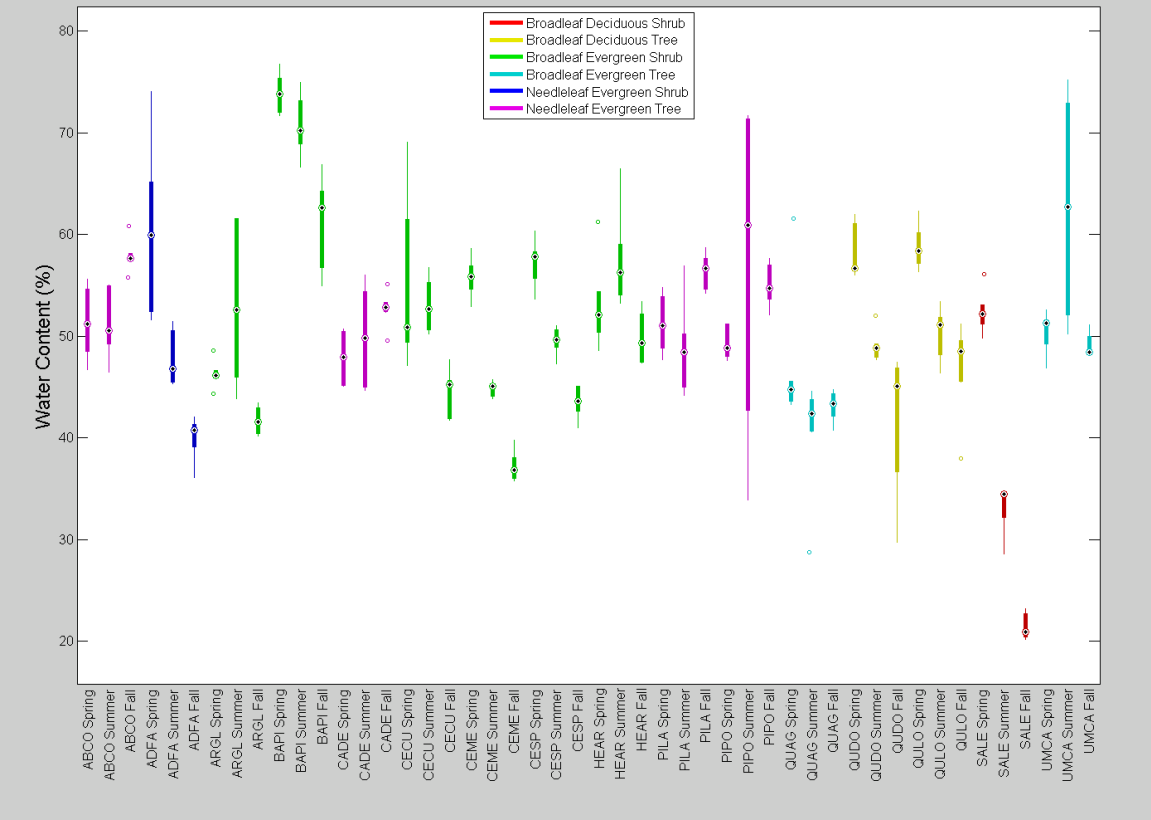

Figure A4. Seasonal distribution of water content for all species.

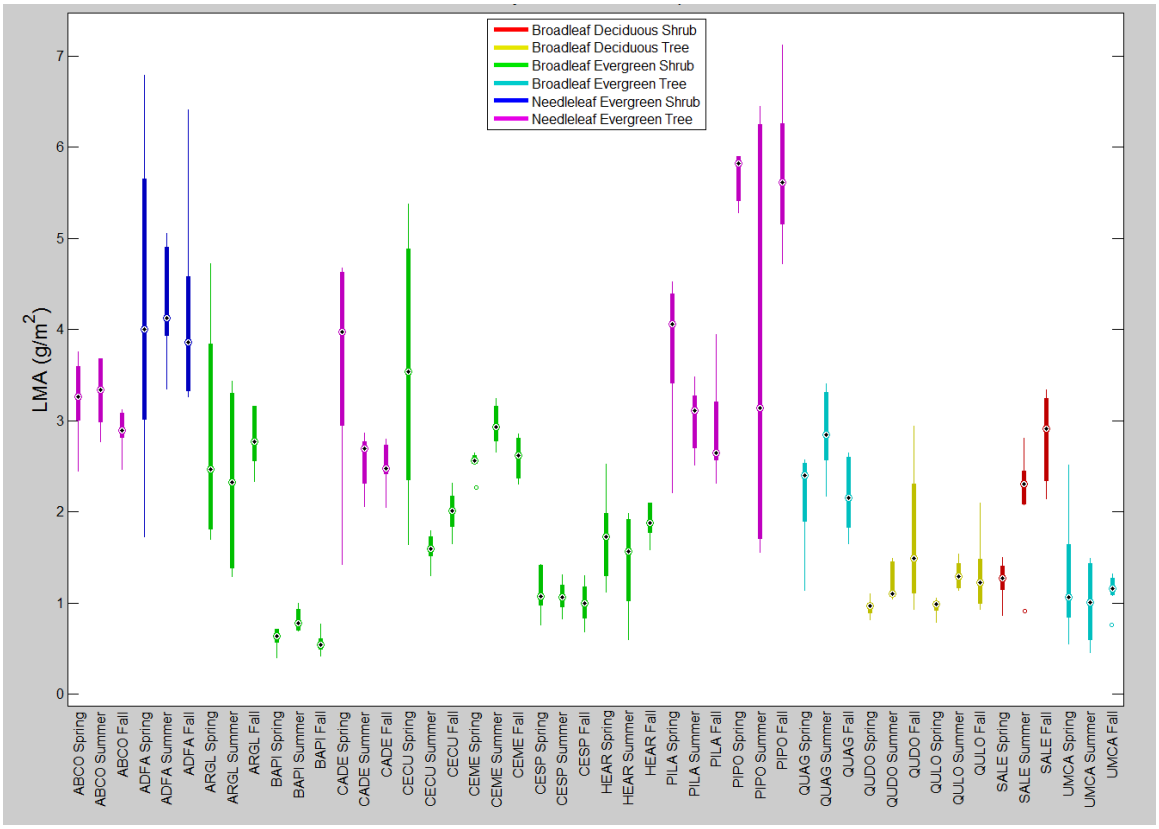

Figure A5. Seasonal distribution of LMA for all species.

Table A1. Statistics for partial least squares regressions (PLSR) for lignin, cellulose, and nitrogen.

		Lignin			Cellulose			Nitrogen		
		R^2	# of Factors	RMSE%	R^2	# of Factors	RMSE%	R^2	# of Factors	RMSE%
All Samples	Full	0.84	18	6.20	0.89	19	6.65	0.81	16	7.52
	VSWIR	0.56	11	8.35	0.95	34	4.64	0.87	25	6.20
	TIR	0.40	6	7.68	0.90	16	6.18	0.74	10	8.20
	HyspIRI	0.58	10	7.63	0.83	18	7.78	0.78	18	7.82
	AVIRIS	0.53	9	7.63	0.93	33	7.78	0.86	26	7.82
	HyTES	0.59	8	8.17	0.60	9	5.48	0.51	7	6.61
Spring	Full	0.83	11	9.12	0.93	16	6.04	0.93	12	6.61
	VSWIR	0.77	10	10.10	0.93	17	6.70	0.84	9	8.61
	TIR	0.74	7	9.36	0.92	11	7.26	0.80	8	9.39
	HyspIRI	0.81	11	9.32	0.80	12	10.22	0.89	11	7.36
	AVIRIS	0.78	11	9.93	0.75	12	11.16	0.85	10	8.31
	HyTES	0.93	10	6.23	0.86	9	8.96	0.77	8	10.00
Summer	Full	0.78	9	8.68	0.90	13	7.36	0.82	12	7.82
	VSWIR	0.80	12	9.52	0.87	13	8.01	0.67	8	9.27
	TIR	0.89	10	6.54	0.97	12	4.22	0.85	7	7.71
	HyspIRI	0.82	12	9.07	0.95	22	5.00	0.64	7	9.64
	AVIRIS	0.84	13	8.78	0.82	13	9.01	0.71	10	8.71
	HyTES	0.87	9	8.25	0.64	7	11.43	0.57	7	10.08
Fall	Full	0.76	10	8.08	0.88	11	7.63	0.69	8	11.35
	VSWIR	0.61	9	9.51	0.90	15	7.00	0.63	7	11.62
	TIR	0.82	7	7.40	0.68	6	10.94	0.90	8	7.43
	HyspIRI	0.67	10	8.98	0.90	15	7.01	0.56	5	11.85
	AVIRIS	0.71	11	8.69	0.86	15	8.01	0.52	4	12.25
	HyTES	0.80	8	7.68	0.26	4	9.45	0.35	5	12.06
Broadleaf Deciduous	Full	0.93	10	6.42	0.76	8	10.71	0.96	11	5.38
	VSWIR	0.86	8	8.97	0.71	8	11.21	0.92	10	7.38
	TIR	0.92	7	6.76	0.75	4	10.86	0.71	4	10.09
	HyspIRI	0.91	10	6.97	0.72	7	11.26	0.90	9	8.35
	AVIRIS	0.90	10	7.73	0.65	7	11.61	0.90	8	8.49
	HyTES	0.82	6	10.02	0.77	6	10.03	0.92	9	7.59
Broadleaf Evergreen	Full	0.73	10	8.46	0.94	17	5.46	0.72	10	9.51
	VSWIR	0.90	23	6.11	0.91	19	6.91	0.81	14	7.76
	TIR	0.79	9	7.74	0.80	9	9.41	0.63	8	9.82
	HyspIRI	0.70	10	9.68	0.89	16	7.59	0.81	16	8.07
	AVIRIS	0.77	16	8.73	0.86	16	8.49	0.79	15	8.28
	HyTES	0.79	8	8.52	0.79	9	9.71	0.40	6	10.25
Needleleaf Evergreen	Full	0.76	11	8.81	0.93	12	6.27	0.63	8	6.22
	VSWIR	0.60	10	8.81	0.96	19	6.27	0.47	5	6.22
	TIR	0.59	4	9.97	0.74	4	10.73	0.89	8	4.70
	HyspIRI	0.57	10	10.50	0.87	12	8.36	0.63	9	6.69
	AVIRIS	0.55	9	10.58	0.98	26	3.32	0.50	5	7.80
	HyTES	0.80	6	8.42	0.88	7	7.90	0.82	6	5.86

Table A2. Statistics for partial least squares regressions (PLSR) for water content and LMA.

		Water Content			LMA		
		R^2	# of Factors	RMSE%	R^2	# of Factors	RMSE %
All Samples	Full	0.92	13	4.59	0.78	12	8.67
	VSWIR	0.91	15	4.66	0.75	12	8.90
	TIR	0.86	12	5.82	0.71	9	9.55
	HyspIRI	0.93	19	4.23	0.75	12	9.06
	AVIRIS	0.90	15	4.23	0.73	10	9.06
	HyTES	0.29	5	4.89	0.52	6	9.19
Spring	Full	0.89	8	7.04	0.83	8	9.46
	VSWIR	0.88	8	7.51	0.83	7	9.14
	TIR	0.97	13	3.26	0.63	6	12.14
	HyspIRI	0.89	9	7.36	0.82	8	9.41
	AVIRIS	0.89	9	7.24	0.82	7	9.47
	HyTES	0.80	8	9.41	0.55	5	12.81
Summer	Full	0.91	10	6.30	0.85	9	7.58
	VSWIR	0.88	7	7.07	0.83	10	7.82
	TIR	0.81	7	8.59	0.89	9	6.36
	HyspIRI	0.89	7	6.86	0.84	10	7.52
	AVIRIS	0.88	7	7.23	0.84	10	7.80
	HyTES	0.55	6	11.21	0.82	8	7.88
Fall	Full	0.87	7	6.45	0.92	12	5.66
	VSWIR	0.86	6	6.51	0.75	7	8.81
	TIR	0.92	8	5.01	0.98	10	3.03
	HyspIRI	0.88	8	6.22	0.72	6	9.21
	AVIRIS	0.85	6	6.91	0.74	7	8.91
	HyTES	0.75	7	8.10	0.48	5	9.89
Broadleaf Deciduous	Full	0.93	9	6.61	0.72	7	11.27
	VSWIR	0.92	8	6.98	0.64	6	9.92
	TIR	0.97	7	4.18	0.88	6	8.13
	HyspIRI	0.91	8	7.16	0.62	3	11.73
	AVIRIS	0.92	8	6.90	0.55	3	11.78
	HyTES	0.99	11	2.68	0.98	11	3.15
Broadleaf Evergreen	Full	0.92	7	5.75	0.82	11	7.63
	VSWIR	0.88	6	6.57	0.77	9	8.33
	TIR	0.74	7	8.69	0.88	12	6.46
	HyspIRI	0.89	7	6.29	0.80	10	7.90
	AVIRIS	0.88	6	6.66	0.77	9	8.10
	HyTES	0.52	6	9.72	0.47	6	10.20
Needleleaf Evergreen	Full	0.90	9	5.46	0.76	10	9.95
	VSWIR	0.86	8	5.46	0.53	8	9.95
	TIR	0.92	6	4.77	0.64	4	10.78
	HyspIRI	0.86	9	6.28	0.56	10	12.04
	AVIRIS	0.86	9	6.33	0.53	8	12.32
	HyTES	0.55	3	8.35	0.66	4	10.43